ADDIS ABABA UNIVERSITY

ADDIS ABABA INSTITUTE OF TECHNOLOGY

SCHOOL OF ELECTRICAL AND COMPUTER ENGINEERING

Speed Control of Switched Reluctance Motor for EVs using FLC-DTC

A thesis submitted to School of Graduate Studies, Addis Ababa Institute of Technology, Addis Ababa University in partial fulfillment of the requirement for the Degree of Master of Science in Electrical Engineering (Control Engineering)

By

Biruk Abebe Derseh

Advisor

Mengesha Mamo (PhD)

June 19, 2025

Addis Ababa, Ethiopia

Addis Ababa University

Addis Ababa Institute of Technology

School of Electrical and Computer Engineering

Speed Control of Switched Reluctance Motor using FLC-DTC based for EV

By: Biruk Abebe Derseh

Approved by Board of Examiners

Name	Signature	Date
Sosina Mengistu (PhD) (School Head)	_____	_____
Mengesha Mamo (PhD) (Advisor)	_____	_____
Mesfin Tilahun (PhD) (Internal Examiner)	_____	_____
Lebsework Negash (PhD) (External Examiner)	_____	_____

Declaration

I hereby declare that this MSc thesis has been composed by myself and that the work has not been submitted for any other degree or professional qualification. All sources of material used for this thesis have been duly acknowledged.

Biruk Abebe Derseh

Name

Signature

Acknowledgement

First and foremost, I would like to express my deepest gratitude to God for giving me the strength and perseverance to complete this thesis. Next, I extend my deepest appreciation to my thesis advisor, Dr. Mengesha Mamo, for his invaluable guidance, constant encouragement, supportive attitude, and patience throughout this journey. Last but not least, I am also profoundly grateful to my family for their unwavering love and support. Thank you all for being my foundation and strength all through my life.

Abstract

Nowadays, the popularity and demand for electric vehicles have increased, and much effort has been devoted to the creation of high-performance EV drives. This is primarily to reduce environmental pollution caused by emissions from internal combustion engine (ICE)-powered vehicles, and to replace fossil fuels with renewable energy sources because of their rapid depletion. Electric motors are the key components of electric vehicles; thus, their selection is important due to their effects on the performance of the entire system. Many types of electric motors have been analyzed and evaluated for the use electric vehicles. Switched Reluctance Motor (SRM) are suitable for high-speed drive application due to the absence permanent magnet and winding in the rotor. SRM have a numerous of advantages over other electric motors due to their robust structure, low cost, ability of fault-tolerant and resilience. In spite of these advantages, SRM suffers from high torque ripple which will result in undesired vibration and acoustic noise. When taking into account the needs of traction application, the most significant and difficult SRM concerns are torque ripple minimization and reference speed tracing. An adequate control scheme is essential for the drive to have a good dynamic and transient response and also to tracks the reference speed while minimizing the ripple torque of the SRM. In this thesis, a fuzzy logic controller is designed to increase system performance by reducing torque ripple and eliminating the speed reference tracking problem. The designed controller enables the actual speed to follow closely with the reference speed in 0.047 seconds. It shows 59.04% and 53.47% improvement in rise time compared to the PI controller and conventional FLC, respectively. Simulation results were obtained using the MATLAB/Simulink environment for the effectiveness of the study.

Keywords: **Electric vehicle, Switched reluctance motor, Direct torque control, Fuzzy logic control, MATLAB/Simulink**

Contents

List of Figures

List of Tables

List of Acronyms

AHB	Asymmetric Half Bridge
AC	Alternative Current
BEV	Battery Electric Vehicle
BLDC	Brushless DC
CE	Change Error
DC	Direct Current
DTC	Direct Torque Control
EV	Electric Vehicle
ER-EV	Extended Range Electric Vehicle
EMI	Electromagnetic Interference
FLC	Fuzzy Logic Control
FCEV	Fuel Cell Electric Vehicle
ESS	Energy Storage System
FEM	Finite Element Method
HEV	Hybrid Electric Vehicle
ICE	Internal Combustion Engine
IM	Induction Motor
IGBT	Insulated-Gate Bipolar Transistor
ITBL	Current Torque Look Table
KWH	Kilowatt-Hour
Kg	Kilogram
LIB	Lithium-Ion Batteries
LSRM	Linear Switch Reluctance Motor
LUT	Lookup Table
mAh	MilliAmpere hour

NiMH Nickel Metal Hybrid

OBC Onboard Charger

PMSM Permanent Magnet Synchronous Motors

PHEV Plug-in Hybrid Vehicle

PI Proportional Integral

RPM Run Per Meter

SRM Switched Reluctance Motor

SVM Space Vector Modulation

TMS Thermal Management System

TTBL Torque Lookup Table

TSK Takagi-Sugeno-Kang

VCS Vehicle Control System

Wh Watt-hours

List of Symbols

B	Rotor damping
β_r	Rotor pole arcs
β_s	Stator pole arcs
e	Back emf
F_r	Rolling résistance force
F_d	Air drag force
F_a	Acceleration resistance force
F_{st}	Gradient resistance force
F_g	Gradient force
g	Gravity
i_{ph}	Phase Current
J	Inertia
L_s	Stator inductance
L_{min}	Minimum inductance
L_{max}	Maximum inductance
m	Mass
θ	Rotor angle
δ	Flux-linkage angle
ω	Rotor speed
λ_{ph}	Phase Flux linkage
λ_0	Initial stator flux
ω_m	Mechanical rotational speed
N_s	Stator pole
N_r	Rotor pole
R_s	Stator resistance

T_e	Electromagnetic torque
T_L	Mechanical load
P	Power
P_r	Rolling resistance power
P_g	Gradient power
P_d	Drag power
u	Control output
V_{dc}	DC voltage
V_n	Voltage state vector
Δe	Change error

Chapter 1

Introduction

1.1 Backround

The globally dominant mode of road transportation relies over internal combustion engine vehicles (ICEs), fueled by gasoline or diesel. However, their extensive use poses a significant and challenging problem. The primary concern surrounding ICE vehicles is their contribution to climate change. ICE vehicles emit greenhouse gases and other harmful substances into the air, contributing to global warming, ozone layer depletion, and adversely impacting human health problems [1]. Although they are exposed to resource depletion and environmental degradation. However, critical analysis is needed to find solutions to those problems. There has been a growing interest in developing and adopting alternative technologies in recent years.

Electric vehicles (EVs) have received mainstream interest due to their immense contribution to the environment and economy. EVs are the way forward for green transportation and for establishing clean energy by reducing the use of depleting energy resources. They contribute numerous benefits by significantly clearly overshadowing the internal combustion engine by lowering pollutants like nitrogen oxides (NOx), leading to lower carbon dioxide (CO2) emission [2]. Also, EVs offer several attractive features of low maintenance, reduced noise pollution, fostering high efficiency, and reduction of transportation charges among individuals [3] [4].

By diversifying energy sources and reducing tailpipe emissions, EVs are capable to improving energy security while safeguarding the environment. As discussed in [5], the reason for Electric vehicles to serve as superior than internal combustion engine vehicles (ICEVs) can be attributed to their electric motor and efficient power train capability.

With great concern for electrification, an essential component of electric vehicles is the electric motor [6]. Different types of motor drives are used as traction motors like DC motors, induction motors (IM), switching reluctance motors (SRMs), and permanent magnet synchronous motors (PMSM). Electric motors with high torque density and low mass are well suited for direct drive applications. Conventional induction and DC motors have dominated the variable-speed electric drive fields due to their robustness and flexibility. A permanent magnet synchronous motor is extensive as a drive for EV applications [7]. Due to the limited availability of rare earth minerals, these drives are more expensive. SRM provided a high-performance drive without the use of these rare earth elements as a promising option. It grasped the eyes of researchers as the best alternative to permanent magnet synchronous motors [8].

Switched reluctance motors are characterized by their simple and robust construction, capability for high speed operation, and benefits such as low cost and high reliability, making them widely utilized in electric vehicles and various other applications [9]. SRMs are demonstrated to be reliable and economical in harsh environments because of the lack of winding enduring magnet within the rotor. However, the torque pulsation is large because of its double salient structure and nonlinear magnetic saturation, which results in poor motor speed control. As a result, SRM's performance needs to be optimized and its accuracy further increased.

There are different power converter topologies exist for the SRM R-dump, C-dump converter, Buck-Boost converters, and asymmetric bridge converter [10]. Speed response, cost, and torque ripples are the primary constraints on converter planning. and controller for SRM. Mainly, the current overlapping is the major issue associated with the above converters. The AHB converter is preferred for applications where simple and precise torque control is required, and it is suitable for high-performance applications.

Fuzzy logic controllers offer the unique advantage of integrating experience, logical reasoning, intuition, and heuristics into the system rather than relying solely on mathematical models [11]. They excel in modeling complex nonlinear functions, providing improved results when handling imprecise data. By leveraging knowledge and experience, fuzzy logic controllers enhance system performance by capturing the underlying characteristics of the system. Intelligent control techniques address uncertainty through the use of IF-THEN rules, which establish relationships between inputs and outputs.

The Direct Torque Control method was first put forth for the induction motor in the 1980s [12] [13]. In comparison to conventional current control methods, the most popular control

method for switched reluctance motors (SRMs) is direct torque control (DTC) which reduces torque ripple. Simple construction, quick dynamic torque response, and reduced machine parameter dependence are only a few benefits of direct torque control. Since this approach chooses the voltage space vector based on the torque and flux linkage errors, there is no need for a current controller.Noise reduction, reduced mechanical vibration, and low torque ripple can all be accomplished with proper torque control in the SRMs.

In performing simulation to evaluate the design system, if the results are suboptimal, modifications are made by adjusting the controller's parameters or refining the fuzzy rules. This iterative process continues until satisfactory results are achieved, all without altering the system design.

For EVs to be appropriate for long-distance travel their batteries must have a high energy density in order to increase the vehicle's driving range. [14]. The extended cycle life, high effectiveness, broad operating temperature, and affordability in commercialization are its meeting requirements [15]. Numerous battery kinds have been produced, such as lithium-ion batteries (LIBs), lead-acid, nickel-based, and sodium-based batteries [16]. [17].Since LIBs have better qualities than the others—such as greater energy density, specific power, recyclability, less weight, longer cycle life, lower self-discharge rates, and quicker charging times—they are the most popular energy device for electric vehicles (EVs) [18] [19].

This thesis work presents the study and design of speed control of SRM using a controller of fuzzy logic control and torque control using DTC to minimize torque ripple for BEV applications. The efficiency of the developed method has been demonstrated through simulations.

1.2 Statment of the problem

Switched reluctance motors (SRMs) are suitable options for high speed performance applications like electric vehicles (EVs) due to their simple design, high reliability, and cost-effectiveness. However, SRM drives face challenges like high torque ripples and acoustic noise, which stem from their doubly salient structure and can negatively impact both motor and vehicle performance and efficiency. While conventional control methods have been used for SRM drives, they struggle to manage the motor's nonlinear and dynamic behaviors. This highlights the need for alternative control approaches that can improve SRM drive speed response and reduce torque ripples for EV applications.

1.3 Objective of the Thesis

1.3.1 General Objective

The main objective of this thesis is to provide a fuzzy logic control that minimizes torque ripple for the electric vehicle application while allowing the switched reluctance motor to track its reference speed.

1.3.2 Specific Objective

This thesis specifically aims to:

- Study a dynamic mathematical model of a 6/4 SRM
- Design FLC
- Reduce torque ripple
- Implement the system in MATLAB

1.4 Methodology

The methodology for meeting the goals relies on a comprehensive review of existing works of literature regarding SRMs, speed controllers, torque ripple mitigation techniques, and collecting data regarding electric vehicles. Establish a brief description of the Mathematical and dynamic modeling of the switched reluctance motor and the electric vehicle dynamics, which are studied and verified using theories. Fuzzy speed control and Direct torque control are designed. to validate the proposed study Simulink model is built and simulated using MATLAB. speed controller using Fuzzy logic control.

1.5 Scope of the Study

The thesis emphasizes the MATLAB Simulink carrying out the speed controller using fuzzy logic control and hysteresis-based flux and torque controllers of switched reluctance motors for propulsion EVs. Furthermore, it uses the direct torque control technique to minimize the function of the high torque fluctuations. comparative studies and analysis are held with PI and FLC to show how well the designed SRM drive

1.6 Relevance of the Study

The study greatly advances the possibility of improving the effectiveness and efficiency of electric vehicles (EVs) through regulating the speed and mitigating the torque ripple of switched reluctance motors (SRMS). The research uses FLCs, a robust solution for non-linear and under varying operational conditions with improved speed response and precision. The research shows that SRMs are a suitable option and are highly competent with other conventional motors. Also, the result gives smoother acceleration and better overall energy management in electric vehicles. Further, this study augments the enhancement of green technology through an optimized electric drive system for the transition into sustainable transportation. Eventually, such work could lead to future studies in the field for building up EVs with a wide range of speed applications

1.7 Outline of the Thesis

This thesis is subdivided into six chapters. In Chapter One, the study is presented, along with a brief overview of the topic and background informations. Chapter Two presents the theoretical foundation, including an overview of electric vehicles (EVs), motor classifications, and comparisons. It also reviews existing literature on speed control for switched reluctance motors (SRMs) and explores torque minimization techniques. Chapter Three focuses on the methodology, detailing the foundational concepts, operational principles, and modeling of the SRM. Chapter Four examines controller design techniques for speed control and torque minimization, with a detailed analysis of the designed controller. Chapter Five discusses the results and provides an evaluation of the performance of the suggested controllers in comparison. Finally, Chapter Six provides a summary of the results and suggests possible avenues for further investigation in the conclusion of the thesis.

Chapter 2

Literature Review

2.1 Chapter Overview

This chapter explores the theoretical background of the classification, the key components of electric vehicles (EVs), and the various electric motors used in EV propulsion. A detailed comparison is made between these motors, focusing on performance and efficiency. Control strategies for Switched Reluctance Motors (SRMs) are reviewed and compared. Additionally, relevant research on SRM speed control, with a focus on fuzzy logic controllers is examined to form a basis for the following sections.

2.2 Electric vehicles and their classification

Electric vehicles are run solely on electric propulsion. In a typical manner, there is a possibility to clarify EVs into five kinds based on the electricity employed as the vehicle energy source. These are namely: battery electric vehicles (BEV), hybrid vehicles (HEV), plug-in hybrid vehicles (PHEV), and fuel-cell electric vehicles.

I. **Battery Electric Vehicle (BEV)**

   These vehicles are fully powered by electricity stored in batteries. High-potential packs of batteries are used to propel the vehicle. BEVs have no internal combustion engine (ICE) or fuel tank. They are capable of being charged through the use of an external power source. Most BEVs make use of bigger packs of batteries because their range is closely correlated with their battery capacity. [20].

II. **Hybrid Vehicles (HEVs)**

HEVs are propelled by an electric motor in addition to an internal combustion engine (ICE). A plug-in charger is not required in HEVs. The electric motor is powered by regenerative braking, which charges the battery while the internal combustion engine (ICE) operates on gasoline or diesel. Because of this method, HEVs have been very efficient in city driving because the engines shut off completely when the vehicles are not moving [21]. The electric motor assists the ICE to improve fuel efficiency and reduce emissions.

III. **Plug-in Hybrid Vehicles (PHEVs)**

The advancement of the HEV with a plug-in charger and increased battery capacity that enables it to recharge the battery from the power grid is known as a plug-in hybrid electric vehicle. [22]. These vehicles, alike Because its primary power source is electric propulsion, HEVs have larger batteries and plug-in capability. They have a short range when powered solely by electricity, and when the battery runs low, they can transition to an ICE vehicle. Either an external power source or the ICE can be used to charge PHEVs.

IV. **Fuel Cell Electric Vehicles (FCEVs)**

An electric motor in a fuel cell electric vehicle is driven by electricity that is generated by a battery and a fuel cell. A fuel cell transforms hydrogen gas, which serves as the power source, into electrical energy [23]. These vehicles need to be refueled with hydrogen at a special station, but it only takes a minute to refuel. Water vapor is the only emission from FCEV.

V. **Extended Range Electric Vehicles (ER-EVs)** vehicles that integrate the attributes of the plug-in hybrid electric vehicle (PHEV) and a battery electric vehicle (BEV) are called extended-range EVs. They can go farther on electricity alone since they have a bigger battery pack than PHEVs. However, a tiny gasoline engine produced electricity and drove the electric motor to increase the vehicle's range in the event that the battery ran out.

2.3 Key Parts of Battery Electric Vehicles (BEVs)

Various subsystems are combined and work together to provide power, control, and safety for the electric vehicle. Some main components such as energy storage systems (ESS), powertrains, power electronics [24], vehicle control systems (VCs), and thermal management systems (TMS).

The four primary subsystems of electric vehicles are the motor driver, traction motor, battery pack, and control units. To maximize knowledge and improve participation in the study, it is essential to comprehend the essential components of an electric vehicle.

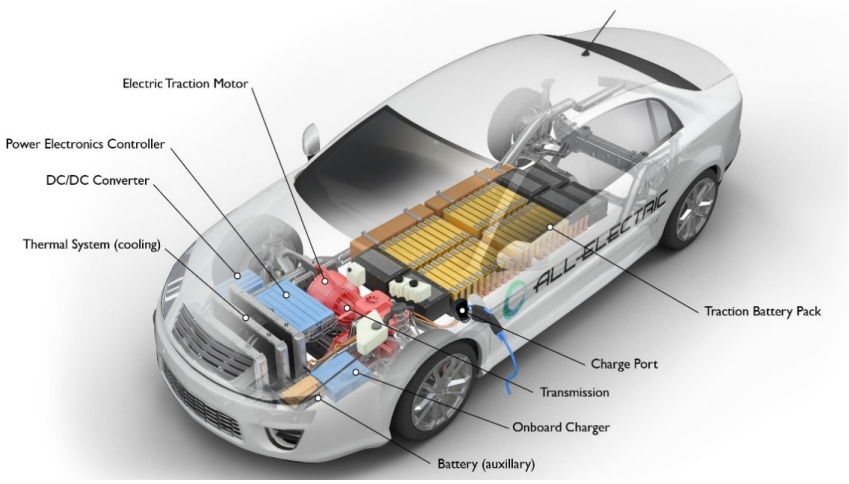

Figure 2.1: vital components of EVs [25]

Auxiliary Battery: provides fixed power necessary for electric vehicle systems and accessories to work.

Traction battery pack: The battery pack is the core component of an electric vehicle. It's made up of numerous lithium-ion battery cells, which store electrical energy. The capacity and density of these batteries determine the car travel range.

Onboard charger (OBC): OBC is mounted inside the electric vehicle which is responsible for charging of EV battery anywhere through a single/three-phase AC supply outlet. Power can be provided by a rectifier followed by DC chopper to control the voltage and current based on the demands of the EV and charge the battery.

Electric traction motor: Electric motors are used in electric vehicles to drive the wheels by electromechanical energy conversions.

Charge port: a port, where the plug-in charger of the vehicle connects to recharge its batteries of traction pack.

DC chopper: widely employed to provide regulated and utilized for the application devices that work in the DC source.

Power electronics: control the electric current from the traction battery pack and the electric motor.

Transmission: Electric cars typically use a single-speed transmission or a simplified multi-speed transmission because electric motors can produce significant torque at low RPMs. Unlike conventional vehicles, there is no need for complex multi-gear transmissions.

2.3.1 Electric vehicle batteries

Batteries are the key source in the electrical system that supplies the motor for vehicle propulsion. High-priced batteries account for half of the entire cost of EV, which makes them expensive. [26] [27]. Electric vehicle (EV) batteries are essential in determining both the performance and driving range of EVs. The energy density of these batteries has an impact on acceleration and overall performance, while power density determines how far a car can go on a single charge, which dictates the distance. Kilowatt-hours (kWh), the battery's capacity, has a direct impact on how much energy is available for driving.

Efficient batteries convert stored energy into power with minimal loss, thus improving performance. Moreover, the weight of the battery impacts vehicle handling and efficiency. Fast charging capabilities and effective thermal management systems are also crucial for maintaining optimal performance and extending the driving range of EVs. Lithium-ion batteries (LIBs), lead-acid, nickel-based, and sodium-ion batteries were among the battery types developed and promoted for electric vehicles. [28] [29] [30] [31].

Nickel metal hydride batteries (NiMH): The size of these batteries is compact and have good power/energy density as compared to other batteries types. Nevertheless, these batteries need regular maintenance and show poor performance at very high and low temperatures, limited service life, and a high self-discharge rate [32].

Nickel-Cadmium (Ni-CD): Batteries perform better in high-temperature operating situations and are appropriate for deep drain cycle applications. They are small and light in weight [33]. However, Due to their poor energy density and significant levels of hazardous metals, Ni-CD batteries are not ecologically benign and are not widely used in EV applications.

Lithium-Ion (Li-ion): The energy density of these batteries is high due to the use of lithium-ion phosphate and Lithium-ion polymer. It has a broad operation with various temperature ranges, the capability of rapid charging, and a relatively long life cycle, which makes it most suitable for EV applications.

2.3.2 Traction Motor

Electric motors perform a crucial function of electric vehicles (EVs) in wheel-driving by electromechanical energy conversion. The recent growing interest in EVs requires a reliable, cheap, and efficient motor drive for propulsion purpose. The major requirements for the selection of motors used in vehicle propulsion are mentioned in the literature and selected based on the below requirements [34] [35] [36]:

- ➢ Torque-speed characteristics (high torque required in low speed for startup and uphill motion; a broad range of speed; including fixed torque and constant region of power; a rapid torque change; a high performance in speed and torque).
- ➢ High power-torque per unit volume, that is, compactness
- ➢ High power density
- ➢ Excellent dependability and durability during a range of vehicle operating circumstances
- ➢ cost-effective
- ➢ Operation within harsh environments such as dust, water, and hot and cold temperatures

Mainly, four types of motors are used in EV applications DC motor, PMSM, IM, and SRM [37]

2.3.2.1 DC motor

Brushed DC Motor Drives: Since they have easy speed control and speed-torque characteristics that meet traction requirements, they have been a popular choice for electric propulsion. Brush DC motors face several disadvantages, including rapid wear and tear due to the friction between the brushes and the commutator. This interaction also causes arcing and electrical noise, which can interfere with other electronic devices. Additionally, the mechanical limitations of the brushed and commutator restrict the maximum speed of these motors Citroen Berlingo is an EV that utilizes the DC machine. However, it has a large heavy structure, low efficiency, and reliability. The need for brush maintenance reduces its competitiveness in the EV market.

Brushless DC Motor Drives: Because of the BLDCM relies on an electronic commutator

rather than a mechanical one, brushless DC motors are reliable with comparing DC motors [38]. Simple structure, high starting and braking torque, robust overload capability, broad speed regulation range, and minimal electromagnetic interference are the primary advantages of BLDCM [39]. However, because of their limited capabilities for field weakening, these motors are naturally constrained to a short constant-power zone.

2.3.2.2 Induction motor (IM)

An induction motor has rugged, simple construction, low maintenance, low cost, and zero cogging torque [40] and is one of the most developed competitors in the EV market. Nevertheless, it has narrow torque-speed characteristics due to its breakdown torque characteristics. Its cooling process is complicated as heat is generated in the rotor copper bars. Also, the IM has low fault tolerance due to magnetic coupling between distributed stator windings. Low efficiency and low power factor, especially at light loads, along with low inverter utilization, are major shortcomings that have yet to be resolved. BMW X5, Renault Kangoo, and Chevrolet Silverado use IM for their traction motors.

2.3.2.3 Permanent Magnet Synchronous Motor (PMSM)

The high power density of the (PMSM), which results from the intrinsic PM excitation, is one of its notable characteristics. With great efficiency, the PMSM provides a broad speed-torque range. As such, it is regarded as the primary traction motor. [41].
The PMSM is adopted as the propulsion motor in the Nisan Leaf, Hyundai Sonata, Honda Accord, and Toyota Prius, which is one of the best-selling EVs. However, PMs are prone to demagnetization, thereby it has low fault tolerance. Due to supply constraints and rising costs for rare earth materials, the market is now forced to look for appropriate substitutes for motors. Ferrite permanent magnets do not represent an alternative to rare-earth magnets. They only offer one-third of the residual flux, can be easily demagnetized, and have a lower torque density than rare earth PMs [42]. Consequently, research is focusing on magnet-free machines.

2.3.2.4 Switched reluctance motor (SRM)

SRMs are a new type of motor. One of its many obvious features is that it has a simpler structure than any other motor. The stator is covered in simple concentrated windings, whereas the motor's rotor is composed entirely of pure (laminated) steel and lacks slip

rings, windings, and permanent magnets. The reluctance motor is suited for use in electric vehicles due to its high starting torque, broad speed range, and strong inherent fault tolerance capability. [43].

SRMs are employed in high-speed applications, within high temperatures, and can operate in harsh environmental conditions [44] [45]. The Holden Commodore is an example of an electric vehicle that utilizes SRM. However, as a disadvantage, the vibration and the acoustic noise are large [46].

2.4 SRMs Overview

Based on the motion's characteristics, SRMs can be broadly divided into two categories: rotational and linear.

i. **Linear switched reluctance motor**

They are intended for linear motion requiring uses and has the feature of a long rotor with a single-step arranged stator. They are used for railway and marketplace machine tools for catering purposes.

ii. **Rotary switched reluctance motor**

A structure exibits double-salience stator and rotor poles and a large output torque in rotary SRM. However, SRM based on rotating machines distinguishes between the radial field and the axial length of the motor. along the magnetic field orientation. Radial field SRM refers to the magnetic field route that runs along with direction perpendicular to the shaft. The motor is referred to as an axial field SRM when the flux path or direction aligns with the rotor's rotation, or axially.

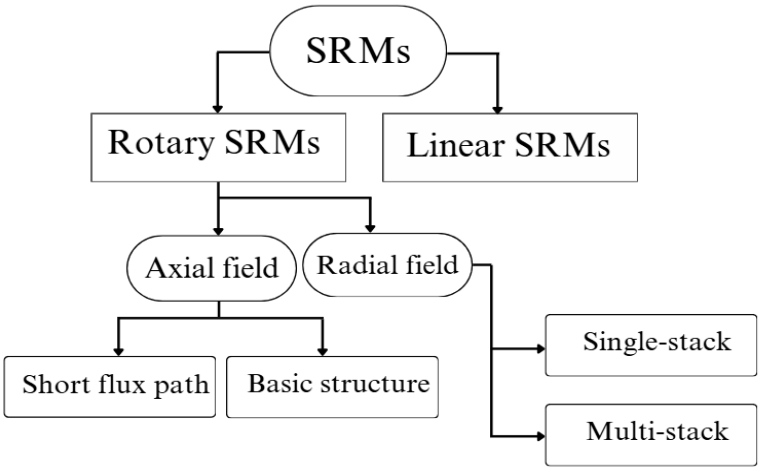

Figure 2.2: Classification of SRMs

2.4.1 Advantages and Disadvantages of SRM

2.4.1.1 Advantages of Switched Reluctance Motor

SRMs have distinct features that position them as a strong rival to the current DC and AC motors in applications requiring high speeds. Switched reluctance motors (SRMs) offer several advantages briefly elucidated as follows:

➢ Simplified Construction:

- SRMs have a stator with only phase windings, whereas the rotor is made of steel laminate and is devoid of permanent magnets and conductors.

➢ Wide speed range:

- As the rotor has no coil on it thus SRM has less inertia and hence can possess the motor's higher speed.

➢ Robustness:

- Due to the rotor being free from of windings and magnets, it becomes highly mechanically robust and can be used for swift operations
- Since the generated torque is precisely proportional to the square of the currents, it is not impacted by the phase current polarity; the current direction is not important.
- Cooling of the SRM is very easy due to the major contribution of losses at the stator windings alone.

➢ Higher efficiency:

- The rotor of an SRM is made of steel lamination with no permanent magnets or conductors, and the stator is made up of solely phase windings.
- As there is no magnet in the rotor, the maximum allowable temperature becomes high. It can be operated in any harsh environment.

➢ Cost savings:

- The rotor of SRMs is made of steel lamination devoid of permanent magnets or

conductors, whereas the stator is made up of solely phase windings., which is low cost compared to other motor types.

- As one of the brushless machines, it provides a superior performance when compared with DC machines from the maintenance point of view.
- SRM requires a simpler cooling system due to the stator side being the primary source of high heat instead of the rotor. The stator is easier to reach than the rotor, making cooling provisioning simpler.
- Since the current corresponds only with the stator windings, heat exists only with the stator, and it can be easily cooled down. Each phase stator winding is separated electrically, which neglects mutual inductance.

➢ Reliability:

- An electrical failure in one phase generally has no effect on other phases since the windings are electrically independent of one another and have very little mutual coupling. The SRM has this particular feature.
- Because the phases are electrically independent, the SRM's inherent flexibility in selecting any number of phases contributes to its excellent dependability in the event that one or more fail while the system is operating.
- Due to their phase independence, SRMs have high fault tolerance. Such feature are not the case for other types of motors This leads to higher reliability of SRM

2.4.1.2 Disadvantages of Switched Reluctance Motor

Although SRMs provide numerous advantages, they are still suffering from some drawbacks:

➢ Torque ripple:

- When compared to other kinds of machines, the double saliency structure and the independent phases' discrete torque production lead to a greater torque ripple.

➢ Acoustic noise and resonant vibration

- The radial electromagnetic force in SRMs varies rapidly, which causes noise and vibration mostly on the stator teeth.

2.5 Related works on Speed controlling of SRMs

Several studies looking into methods and algorithms to control switched reluctance motor speed have been published.

In [47], Presents the study and analysis of the PI-based SRM. The researcher performed a comprehensive investigation and simulation under different conditions. The designed controller minimizes torque fluctuation using current and speed regulation and the simulation verifies their theoretical relation. It emphasize the capability of the motor to replace induction motors with its simple design and Cost-effectiveness. However, the analysis does not address the advance of transient responses. In [48], the PID controller has been applied to accomplish the least time domain of ISE for controlling the motor speed and the PSO algorithm is employed to identifies controller parameters. It is implemented on MATLAB/Simulink and shows robust results.

A study in [49], has proposed the fast terminal SMC speed control method. A comparison study is held in the intended study with PI and conventional SRM, which significantly shows the designed controller behaves finite-time and quick response in reference speed tracking with load disturbance. A chattering effect existential and further study need.

Non-linear systems can modeled easily using linguistic variables in FLC. The authors in [50], proposed the FLC current control and compared with traditional hysteresis current control, shows tolerance for inconsistent switching frequencies. FLC is employed to maintain the current of the motor to follow its reference. The generated error in the current and the change is fuzzified with triangular MF transformed to linguistic variables and 81 rules used to maps for output actions. The Center-of-Area is used to convert this output into crisp PWM control. Minimum current ripple and torque fluctuation is obtained in the study. However the work conducted is applicable solely to lower-speed (1000RPM) SRMs.

Comparative analysis and design of FLC studied in [51]. The study indicated that the FLCs adjusted a set of voltage variance by tracking the output voltage of the converter and evaluating with reference to generate an actuating signal. simulation performed and shows comparison result between FLC and PI regarding speed, torque, and current. The analysis finalizes the designed controller provides minimal torque ripple and diminished steady-state errors. However, the controller robustness under load variation and parameter change are not adequately explored.

A study has been present in [52], utilised the FLC to regulate the motor speed. The SR motor behavior analyse and demonstrated in MATLAB/Simulink. The study result showed that comparsion with typical PID controller, under loaded conditions, the proposed controller outperformed well for a various speed and had lower speed fluctuation. The researcher assumed SRM drives normally function and outlined the genetic algorithm for improved speed controlling.

Chapter 3

METHODOLOGY

3.1 Chapter Overview

The chapter comprehensively shows several methods by which the thesis was realized, explores the theoretical frameworks, and provides an in-depth study of the mathematical and dynamical modeling procedures of the switched reluctance motor. In addition, vehicle dynamics are analyzed and conducted. Besides the optimal computation of battery of the vehicle detail conducted and designed.

3.2 Outline of the Method

The following strategies and methods are employed to achieve the general and specific objectives. Closely interrelated works are reviewed first. After that, the 6/4 SRM mathematical model is in-depth studied. Afterward, the torque control technique is designed using a direct torque control. The fuzzy logic controller is then made to regulate the motor speed. Later, the proposed system is integrated from both FLC and DTC using MATLAB software. After that, an analysis and evaluation of the system's simulated performance are conducted. The overall flow structure of the thesis is depicted in Figure 3.1.

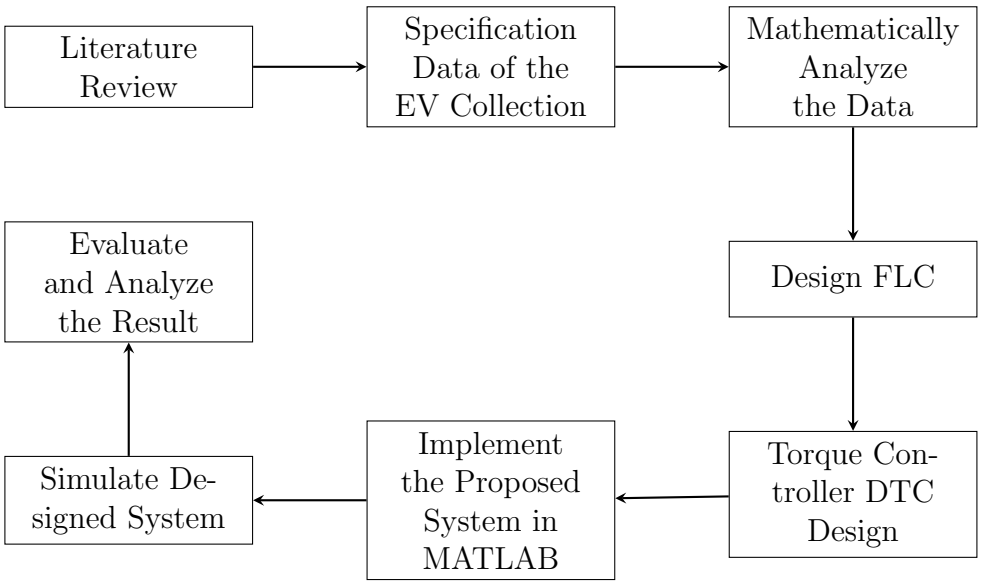

Figure 3.1: Block diagram for the general flow of the thesis

The general block design for the fuzzy logic controller speed controller of the SRM is displayed in Figure 3.2. Two loops are used: the inner loop regulates torque to reduce ripple, and the external loop employs FLC to regulate the motor's speed.

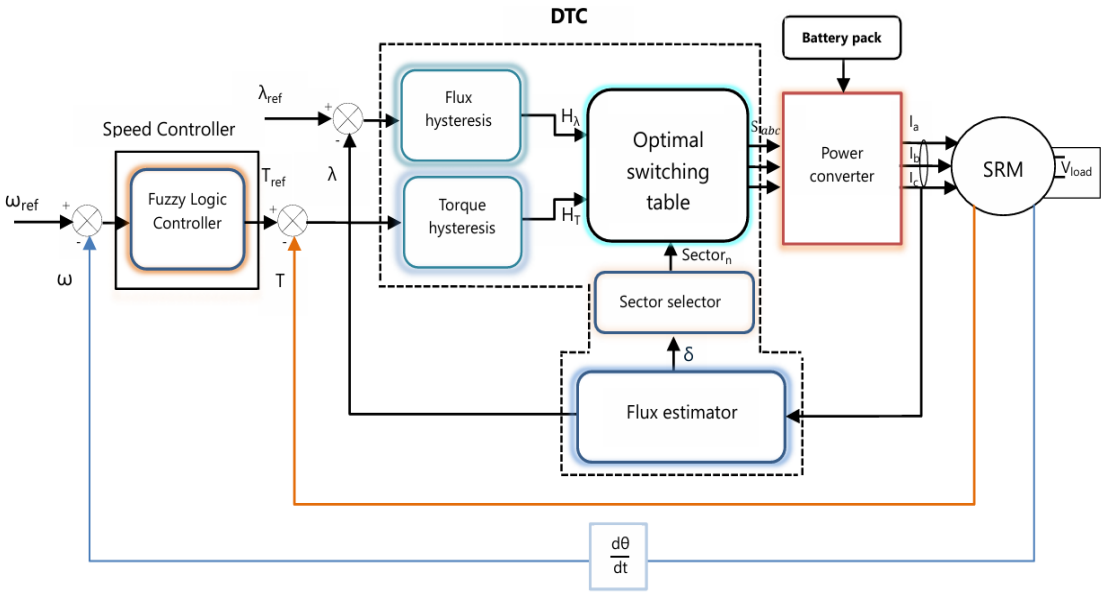

Figure 3.2: Schematic diagram for the proposed system

To control the speed of SRM, the reference speed ω_{ref} is compared with the actual speed ω, thus the generated error is fed to the speed controller. A fuzzy logic controller is employed as a speed controller. It receives speed error as input, and its output is torque. This torque (T_{ref}) is compared with the motor torque within a two-level comparator. FLC is used as a nonlinear function approximation, producing a suitable change to keep the speed. in its reference.

DTC consists of a flux estimator, a switching table, and a three-level torque and two-level flux controller. Using the lookup table, the torque is determined and the flux is approximated using the three-phase SRM model. Based on the sector in which the stator flux is placed, the torque and stator flux demands by the torque and flux comparator, respectively, an ideal voltage vector is selected. Optimal switching vector look-up table selection for every feasible stator flux linkage space vector position. Which region is excited determined by the flux vector depends on the angle of the computed flux.

3.3 SRM Basic Features

Switched Reluctance Motors (SRMs) are known for their simplicity, consisting of stator winding coils that are concentrated on the prominent stator poles and the steel laminate stack rotor that voids magnets and winding in their salient poles. Typically, the stator coils are distributed over the opposite diametrically stator poles and make a series one phase [53]. They are excited in sequence to produce continuous rotation of the rotor.

SRMs are identified by N_s for the stator poles, N_r for the rotor poles, and (m) for the number of phases, where the phases (m) are given by the number of stator pole pairs (i.e., $m = \frac{N_s}{2}$). The motor geometry consists of arcs of the rotor poles β_r, and β_s arcs of the stator pole, which describe the paths of the flux, determining the inductance changing of regions, and how much torque the motor can generate in the phases. The motor is referred to N_S/N_r pole numbers in SRM conventional naming. A three-phase, 6/4 pole SRM cross-section is shown in Figure 3.1.

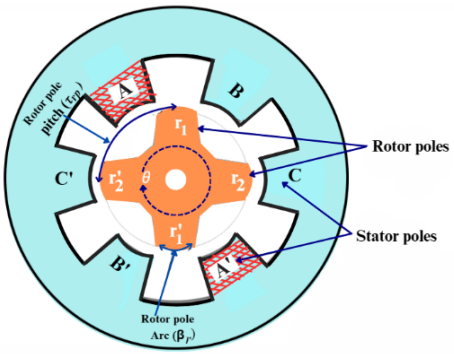

Figure 3.3: Geometric structure of 6/4 SRM

The six salient stator poles are configured with phase per two poles and with four salient rotor poles. The windings in the stator are arranged and equally distributed in the circumference of the motor and are grouped to form three phases.

The phases and number of rotor poles determine the required number of "strokes," or excitation cycles, of a stator phase coil pair for a single complete rotation of the rotor, as illustrated by Equation 3.1. For a 6/4 SRM with a 30° stroke angle per phase. Which shows the angular distance that the rotor moves during one phase excitation cycle as Equation 3.2

$$S = mN_r \tag{3.1}$$

$$\varepsilon = \frac{1}{m}\frac{2\pi}{N_r} \tag{3.2}$$

$$\tau_{rp} = \frac{2\pi}{N_r} \tag{3.3}$$

where S, m, ϵ, τ_{rp} represent the strokes, phases, stroke angle, and rotor pole pitch respectively.

The parameter of the rotor pole pitch is important uses in the design for SRMs, representing the angular displacement between adjacent rotor poles, as defined by Equation 3.3 This parameter profoundly influences torque generation, magnetic flux alignment, and motor operation efficiency.

3.4 Principal Operation of 6/4 SRM

A switched reluctance motor operates by the minimum reluctance principle. The nearest rotor poles are pulled to the location with the lowest reluctance when the winding on a pair of stator poles is turned on. The torque generated by this attracts and the rotor align to the minimum stator reluctance.

If the rotor teeth are in an intermediate position between opposition and conjunction, and if a current is imposed in a phase of the stator, then the teeth of the rotor will move toward a stable position. They will thus be positioned at the conjunction. The minimum magnetic reluctance in the rotor generates a force that tries to align the rotor pole with the closest stator pole when energizing the stator.

Figure 3.4 presents a 6/4 SRM cross-sectional perspective. Smooth rotation will be achieved by providing the appropriate current to each phase winding at the corresponding rotor angle. The excitation occurs sequentially, transitioning from one phase to the next as the rotor rotates.

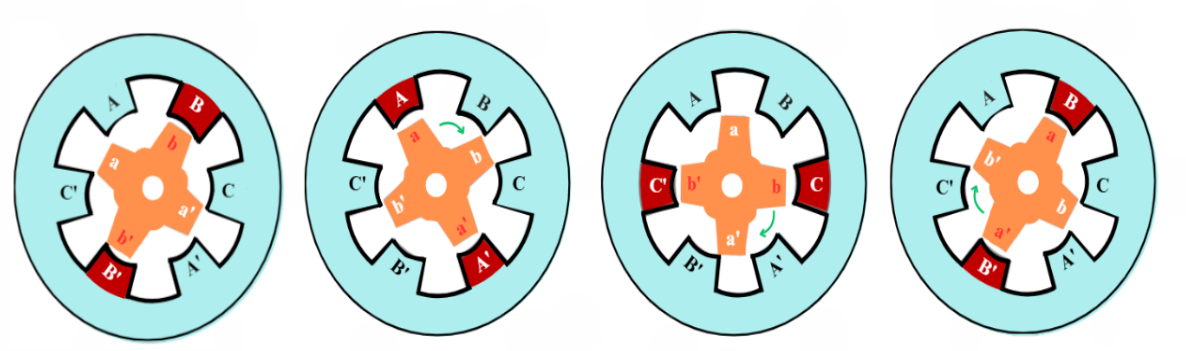

Figure 3.4: Operation of 6/4 SRM

Assume b and b' are the rotor poles are perfectly oriented to the B and B' stator poles illustrated in Figure 3.4-(i). The phase current cannot generate any phase torque in the aligned position. Due to the coincide of those poles, switching action de-energizes the first phase B.

When a current is applied to the stator phase winding A, flux is determined by means of poles A and A' of the stator. A and A', and it causes a force that pulls the rotor pole a and a' towards stator poles as demonstrated in the Figure 3.4-(ii).

Once the poles are aligned, the phase A stator current turns off, then the coil of stator C and C' is energized, pulling b and b' towards the nearby stator pole clockwise, as depicted in Figure 3.4-(iii). The continuous A-C-B excitation sequence of SRM produced the torque to rotate in clockwise.

3.5 SRM Characteristics

3.5.1 Relation between Inductance and rotor position of 6/4 SRM

A switched reluctance motor inductance depends with rotor position and begins to rise as the rotor poles get closer to the stator poles. As the phase inductance rise and fell, the positive and negative torque generated. Figure 3.5 demonstrates the optimal change in phase inductance with the rotor's location for a switched reluctance motor.

When the stator winding of the motor is activated, torque is generated. Consequently, the stator pole draws the closest rotor pole into alignment in the minimum reluctance region and maximum inductance [54]. Current direction does not affect the torque direction, is just dependent on $\frac{dL}{d\theta}$.

Four regions can be identified from the graph given in the Figure3.5 and detailed briefly below:

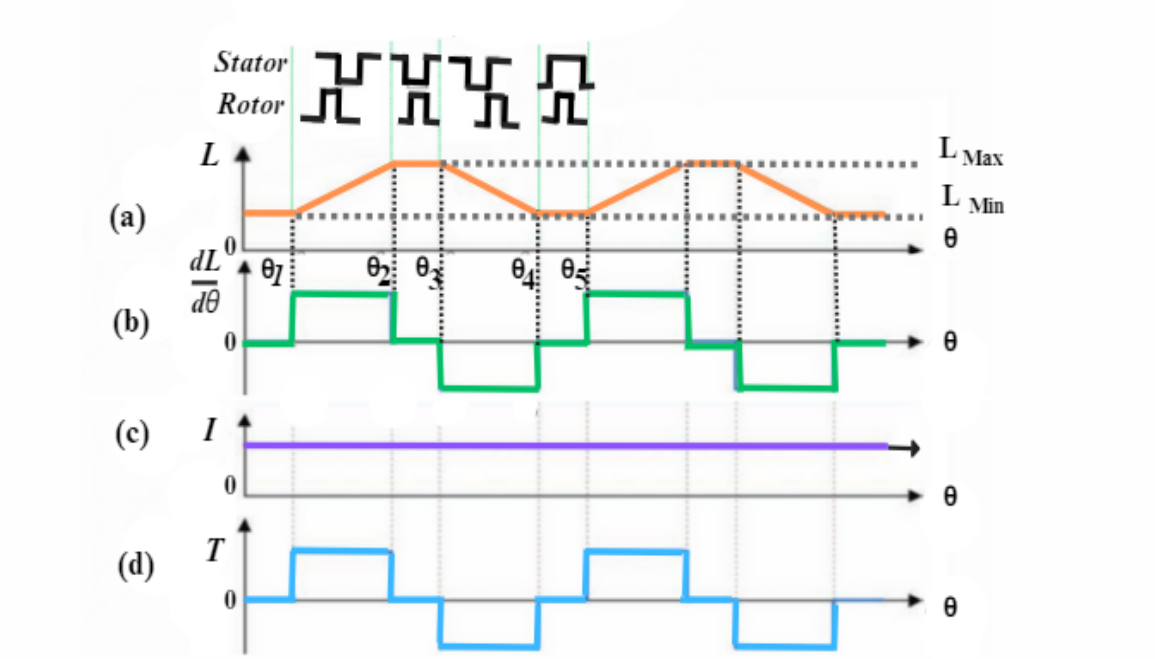

Figure 3.5: Ideal constant excitation characteristics: (a) phase inductance, (b) inductance profile, (c) phase current, and (d) phase torque

I. **Region 1 (0 - θ_1, θ_4-θ_5):** Both the rotor and stator poles are not overlapped in this section called an unaligned position. Flux in this region is obtained through an air gap, which results in the highest reluctance or least inductance. Therefore, torque production is not held in this region. The value of the inductance is minimum and denoted by 'L_{min}'.

II. **Region 2 (θ_1 - θ_2):** The inductance increases linearly with rotation when the rotor leading edges touch the poles of the stator, and this process halts once poles fully overlapped in θ_2. As a result, the inductance rises and becomes positive. A positive torque is produced when a current is applied to the coil at this area. When the pole overlap is finished, this area comes to an end.

III. **Region 3 (θ_2 - θ_3):** During this period, both stator and rotor poles are completely overlapped, then it is called an aligned position, and the phase inductance reaches its maximum and remains constant at this point, which is also called the maximum inductance (L_{max}), and the least reluctance position is reached. Since the inductance remains unchanged, there is no torque generation in this region even with excited stator pole.

IV. **Region 4 (θ_3 - θ_4):** In this area, the rotor separates from the stator pole (the overlap is complete), begins to decrease, and keeps going until $\theta_1 - \theta_2$. except that the inductance

decreases during the rotor position increase, thus causing the region's inductance to slope negatively. When the machine operates in this area, a torque negative occurs, meaning that the variable reluctance machine acts a generator.

Thus, from the above discussion, if the stator is excited in the positive inductance region when operating in motoring mode, the motor contrary to in the area of negative inductance when the stator is excited, the motor works in the regenerative. The summary of SRM Torque production as a function of inductance variation is given in Table 3.1

The rate of change of inductance with rotor position is approximated in a linear piecewise function as:

$$\frac{\partial L}{\partial \theta} = \begin{cases} \frac{L_{\text{Max}} - L_{\text{Min}}}{\theta_2 - \theta_1} & \text{if } \theta_1 \leq \theta < \theta_2 \\ \frac{L_{\text{Max}} - L_{\text{Min}}}{\theta_4 - \theta_3} & \text{if } \theta_3 \leq \theta < \theta_4 \\ 0 & \text{elsewhere} \end{cases} \tag{3.4}$$

Here, the relevant defining positions for the ideal SRM are given as follows:

$$\theta_1 = \frac{1}{2}\left[\frac{2\pi}{N_r} - (\beta_r + \beta_s)\right] \tag{3.5}$$

$$\theta_2 = \beta_s + \theta_1 \tag{3.6}$$

$$\theta_3 = (\beta_r - \beta_s) + \theta_2 \tag{3.7}$$

$$\theta_4 = \beta_s + \theta_3 \tag{3.8}$$

$$\theta_5 = \theta_4 + \theta_1 = \frac{2\pi}{N_r} \tag{3.9}$$

Where β_r, β_s, and N_r are rotor pole arcs, the stator arc and rotor pole respectively.

Table 3.1: Summary of SRM torque production as a function of inductance variation

Rotor Angles	**Alignment**	**Inductance Gradient**	**Generated Torque**
$0 - \theta_1$	Non-coincident	$\frac{dL}{d\theta} = 0$	No torque
$\theta_1 - \theta_2$	Coincident	$\frac{dL}{d\theta} > 0$	+ve torque
$\theta_2 - \theta_3$	Non-coincident	$\frac{dL}{d\theta} = 0$	Zero torque
$\theta_3 - \theta_4$	Misalignment	$\frac{dL}{d\theta} < 0$	-ve torque
$\theta_4 - \theta_5$	Non-coincident	$\frac{dL}{d\theta} = 0$	No torque

3.5.2 Flux Linkage-Current Characteristics of SRM

The flux linkage of SRM is characterized by rotor position and current as nonlinear functions due to hysteresis and nonuniform airgap [55].

The curve of magnetization is obtained utilizing the finite-element method (FEM) [56]. Based on the SRM's physical dimensions and properties. Typically, this computation requires the following information: rotor and stator pole arcs, length of air gap, lamination dimensions, magnetic properties, stator winding size, and number of turns. However, the manufacturer does not provide these building instructions unless you design SRM yourself.

The second method is measuring the curves of magnetization based on the flux equation, a direct method of measurement called experimental measurement [57]. For every rotor position value, the one winding of the stator is subjected to a voltage source. And then the curvesares obtained from the noted current and voltage. This procedure takes a long time and requires a unique setup.

Analytical approximation is the last method of obtaining the curve. Analytical functions use normally available or readily measurable parameters. Calculating the curves using the primary parameters that are often accessible or readily quantifiable would be both practical and preferred.

Due to the motor's nonlinear nature and doubly salient structure, the motor has a tendency to become saturated. Thus, it is difficult to estimate the SRM flux linkage features. Figure 3.6 displays the SRM magnetization curves. Each curve corresponds to a certain rotor angle value that fluctuates between the aligned position (the highest curve) and the unaligned position (the lowest curve).

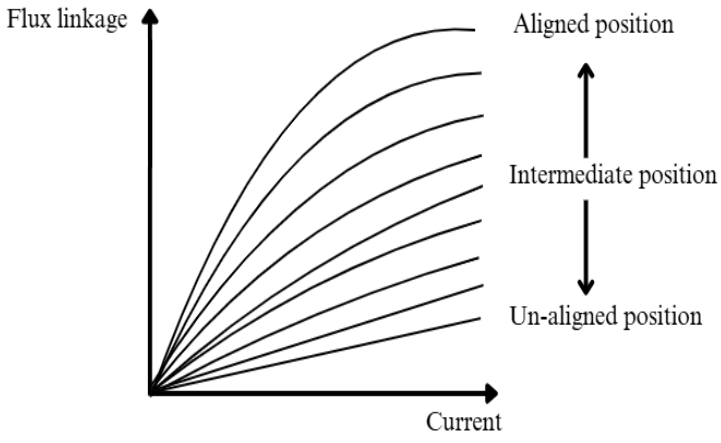

Figure 3.6: Ideal flux linkage characteristics of SRM

3.5.3 Torque Current Rotor Characterstics

The Interaction between torque production and current provided to a switched reluctance motor at various rotor positions is depicted in Figure 3.7. This is called the static torque curve. It can be obtained from a curve of co-energy as a rotor angle function with different current values integrating numerically the magnetization [58].

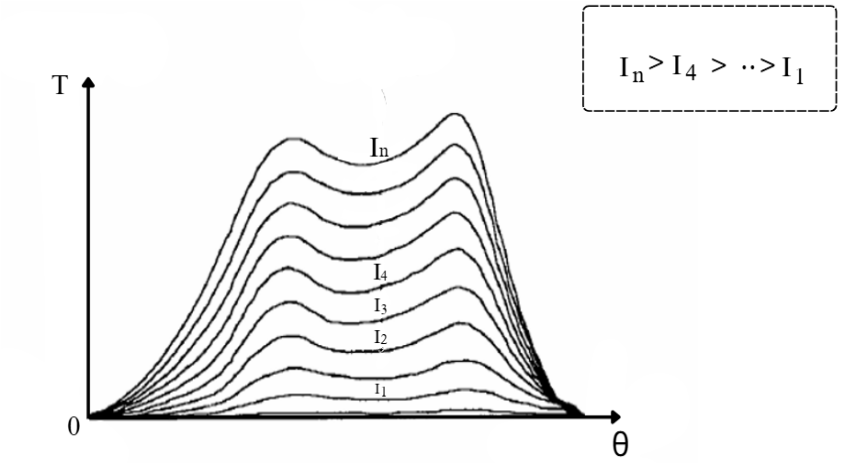

Figure 3.7: Torque current rotor characteristics of SRM

The phase torque SRM is directly proportional to the current squared of the current. During the current increase, the torque initially rises rapidly to reach its peak. After reaching its peak, the torque of the motor slightly decreases due to magnetic saturation.

3.5.4 Speed Torque Characteristics

According to the ranges of varying speeds, Figure 3.8 illustrates how the generation torque can be divided into three distinct regions: the power drop region, the constant torque region, and the constant power region.

Region I: The area below the base speed is the first distinguishing feature, that is the constant torque region. ω_b is the fastest speed at which the nominal voltage may produce the greatest torque and current. The lowest speed at which the motor can run at its rated power is known as the base speed. The phase current's amplitude can be changed to sustain operation in this area. The torque varies with the square of the current, and the flux is proportional to the voltage at a certain speed.

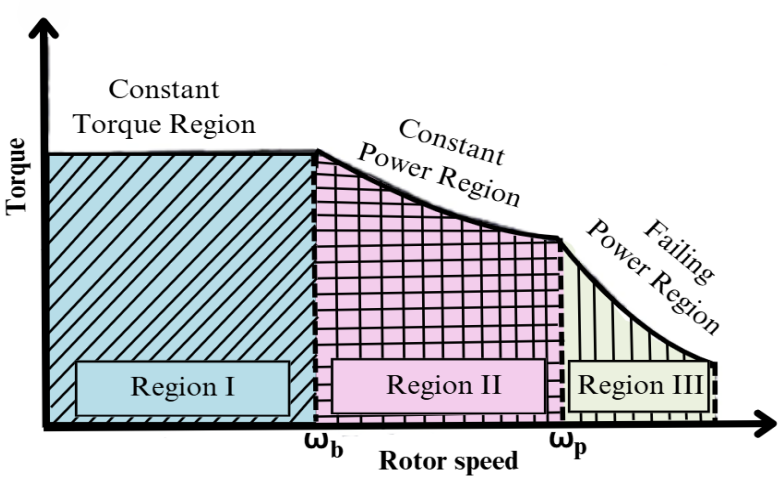

Figure 3.8: Speed-Torque characteristics of SRM

Region II: Controlling the motor on speeds higher than the basic speed is done in the second area. the inherent feature of the SRM while it is running at a fixed supply voltage and various switching angles. Both the torque and the flux are proportional to the square of the current and flux, respectively. In this, the average current delivered to the phase is reduced, the motor speed rises above the base speed, and a steady voltage is applied across the winding until the turn-off angle. A certain point is reached when the current pulse takes up half of the inductance cycle for each phase as the conduction angle increases. In this area $T \propto 1/\omega$, the torque and speed are inversely related.

Region III: The third region is the high-speed range, which consists of switching fixed angles and constant supply voltage. Increasing the angle of conduction is limited in practice. Each pulse ends with a non-zero flux level because the angle of turn-off matches the turn-on angle for the subsequent cycle. The phase winding's net flux rises in this scenario until saturation. This corresponds to a rotor speed. Motor running above this speed implies a fall in torque production as $1/\omega^2$.

3.6 Modelling of SRM

3.6.1 Mathematical Modeling

SRM operates on the least reluctance principle; wherever the reluctance is minimal, the flux path closes [59]. Because of the saturation in depth of the magnetic circuit, the non-uniform distribution of flux at the motor's end, and the non-linearity of the flux density, the parameters of the motor phase winding's flux, inductance, and current will vary periodically with the rotor position angle θ and exhibit a nonlinear relationship.

The SRM's linear analytical model can be expressed using differential equations for electromagnetic torque, voltage, and flux. The electromagnetic field theory explains how the electrical, magnetic, and mechanical energy of SRM are related.

The following presumptions are made in light of the 6/4 SRM case: Each phase is similar, the eddy current is neglected, and there is constant phase resistance.

3.6.1.1 Voltage equation

Each phase is independently excited, and all of the phases have the same structure. Consequently, as the phases change, resulting mathematical equations remain the same and express a single phase.

SRM each stator phase voltage is determined by adding the voltage drop in resistive and the flux linkage's rate of change, as shown in Equation 3.10

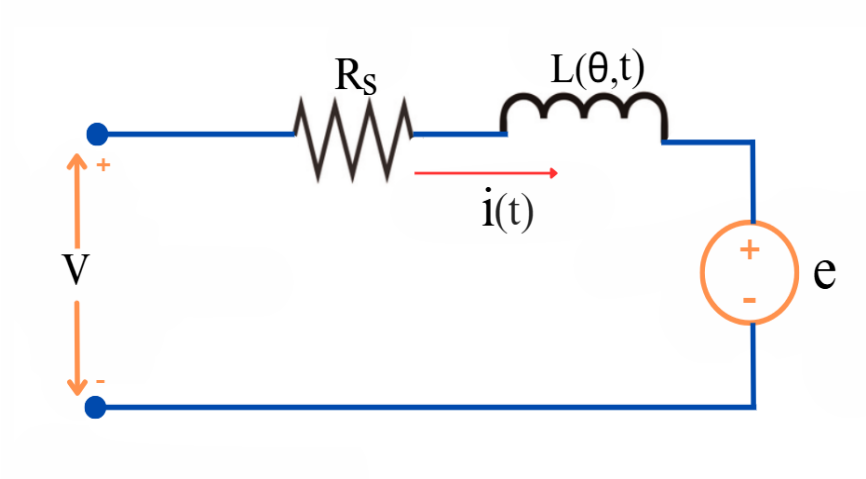

Figure 3.9: SRM equivalent circuit per phase

$$v_{ph} = R_s i_{ph} + \frac{d\lambda(i_{ph}, \theta_{ph})}{dt} + e \tag{3.10}$$

Where v_{ph}, i_{ph}, R_s, λ_{ph}, and θ_{ph} are phase voltage applied to the converter, current, stator resistance, flux linkage, and position of the rotor angle per phase respectively. Since variations in the rotor position and phase current affect the flux value, Equation 3.10 can be modified to provide the following formula, which illustrates how the applied voltage, flux-linkage, and position are interrelated:

$$v_{ph} = R_s i_{ph} + \frac{\partial \lambda}{\partial i_{ph}} \frac{di_{ph}}{dt} + \frac{\partial \lambda}{\partial \theta_{ph}} \frac{d\theta_{ph}}{dt} + e \tag{3.11}$$

3.6.1.2 Flux equation

The flux equation is described using the current and inductance relationship:

$$\lambda\left(i_{ph},\theta_{ph}\right)=L_s\left(i_{ph},\theta_{ph}\right)\cdot i \tag{3.12}$$

where $L_s(i_{ph},\theta_{ph})$ is the stator phase voltage self-inductance
Equation 3.12 being substituted with Equation 3.11 to get

$$R_s i_{ph}+L_s\left(i_{ph},\theta_{ph}\right)\frac{\partial i}{\partial t}+i\omega\frac{\partial L_s\left(i_{ph},\theta_{ph}\right)}{\partial\theta} \tag{3.13}$$

The mechanical speed in Equation 3.13 is determined by the rotor position change with time $\omega=\frac{\partial\theta}{\partial t}$. Consequently, the phase voltage is made up of three parts: the induced back electromotive force (back-emf), the phase inductance's voltage drop, and the resistance's voltage drop.
Equation 3.14 emphasizes how the speed perceived directly is related with back emf:

$$e=\omega i\frac{\partial L\left(i,\theta\right)}{\partial\theta} \tag{3.14}$$

$$v_{ph}=R_s i_{ph}+L_s\left(i_{ph},\theta_{ph}\right)\frac{\partial i}{\partial t}+e \tag{3.15}$$

3.6.1.3 Torque equation

The generated electromagnetic torque of the motor in the independent phase is the rate of co-energy with the angular state of the rotor given by the expression:

$$T_{ph}=\frac{\partial W_c\left(\theta,i\right)}{\partial\theta}\quad\text{where}\quad i=\text{constant} \tag{3.16}$$

Where T_{ph} is the phase torque, and W_c is the co-energy of the magnetic in the phase winding. The magnetic field co-energy W_c described under the area of the curve is:

$$W_c=\int_0^{i_{ph}}\lambda\left(i_{ph},\theta_{ph}\right)\,di \tag{3.17}$$

where i and λ are the current and flux-linkage respectively.
Substitute Equation 3.17 into Equation3.16 and then the familiar simplified relationship for SRM torque T is obtained as:

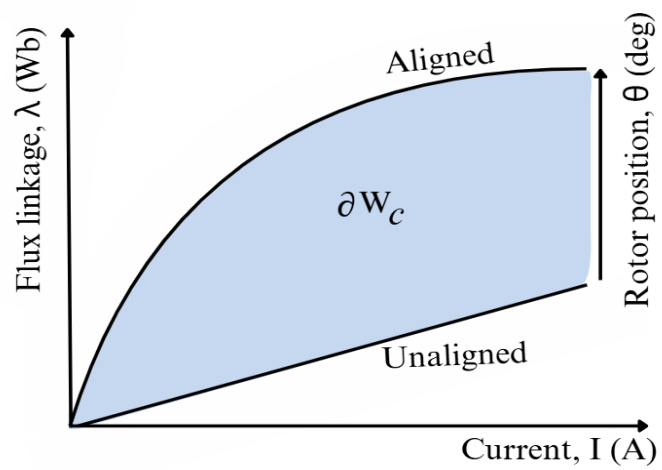

Figure 3.10: Flux linkage-current characteristics

$$T_{ph} = \frac{\partial W_c\left(\theta, i_{ph}\right)}{\partial \theta} = \int_0^{i_{ph}} \frac{\partial L_{ph}\left(i_{ph}, \theta_{ph}\right)}{\partial \theta} i_{ph}\, di_{ph} = \frac{1}{2} {i_{ph}}^2 \frac{dL}{d\theta} \tag{3.18}$$

Where $\pm\frac{dL}{d\theta}$ indicates the motoring/generating modes. As a result, the current and the change rate of inductance change determine the produced torque.

The SRM torque's direction is independent of the current's direction and is determined by the inductance curve's trend. The three-phase SRM total generated instantaneous torque is obtained over integrating:

$$T_e = \sum_{k=1}^{m} T_{ph}(k) \tag{3.19}$$

Where T_e is the total generated torque (electromagnetic torque) and k is the phase number of the motor.

3.6.1.4 Electromechanical equation

The electro-mechanical equation governing the motor behavior is defined as follows:

$$T_e - T_L = \frac{J\, d\omega}{dt} + B\omega_m \tag{3.20}$$

where T_e, T_L, J, B, and ω_m are the rotor torque (electrical torque), mechanical load, system inertia, rotor damping, and mechanical rotational speed respectively.

3.7 Dynamic Modeling of SRM

The primary objective of modeling the motor is to obtain and express the non-linear function with the mechanical output (T, ω) and the input of electrical (V, i). The torque of conventional motors can be expressed as the motor current and its components. In contrast, SRM motor torque depends nonlinearly on the rotor's angular position and phase current. Additionally, the rotor angle and flux linkage affect the phase current.

It is necessary for the SRM model to sufficiently and accurately depict both static and dynamic performances [60]. [61]. The equation of voltage, the equation of torque, and the equation of mechanics consist in the dynamics of reluctance motors. The electrical model for one phase and mechanical sections are configured in the modeling of SRM and depicted in Figure 3.11.

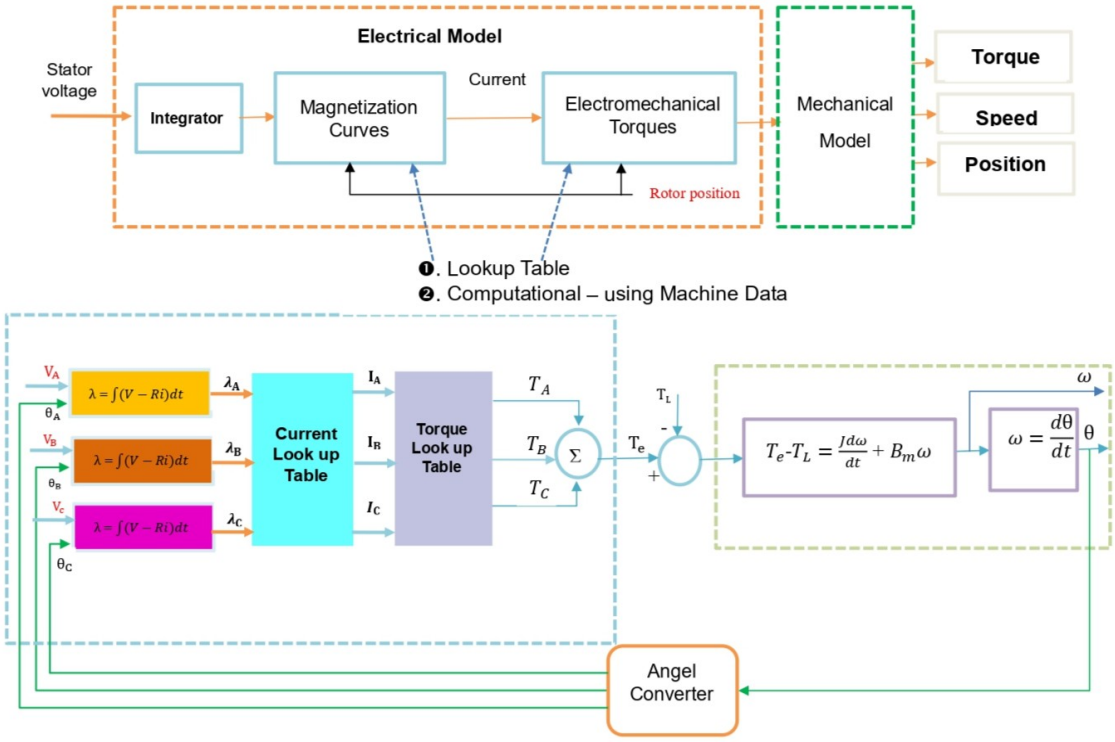

Figure 3.11: Dynamic model of SRM

SRM has its operating principle Considering the variation of reluctance and highly non-linear characteristics. Therefore, it is not usual to model this motor through an equivalent circuit as done for other motors. The most common way to model this type of model is through LUT tables (look-up tables) that show the torque and flux profiles in relation to the rotor position and current information.

$$\lambda_j = \int (v - ri)\, dt \tag{3.21}$$

For the model to work, magnetization and torque characteristics must be acquired. The phase voltages are inputs for the SRM model, and Equation 3.21 is used to obtain the flux-linkage. The magnetization characteristics λ (i, θ) calculate the non-linear stator current i (λ, θ).

Based on the torque characteristics and flux linkage determined by FEA, look-up tables are created from the machine model. The flux-linkage characteristics table includes flux values for various rotor locations and current levels. The torque characteristics table shows torque values for various rotor locations and current levels. The torque, current, and angle (T-i-θ) lookup table is called TTBL, while the flux, current, and angle (λ-i-θ) lookup table is called ITBL.

The total of the individual torques produced in each phase is the SRM electromagnetic torque. Because the magnetization curves are not linear, the generated torque is a non-linear function of the rotor position and current.

3.8 SRM Simulink Model

With MATLAB/Simulink, the dynamic, electromechanical, and linear modeling of SRM is theoretically implemented[62]. There are two tables that exist from magnetization data as depicted in Figure 3.12. Table of current (ITBL) used in the mode circuit and the torque table (TTBL) get the touch electromechanical for each phase.

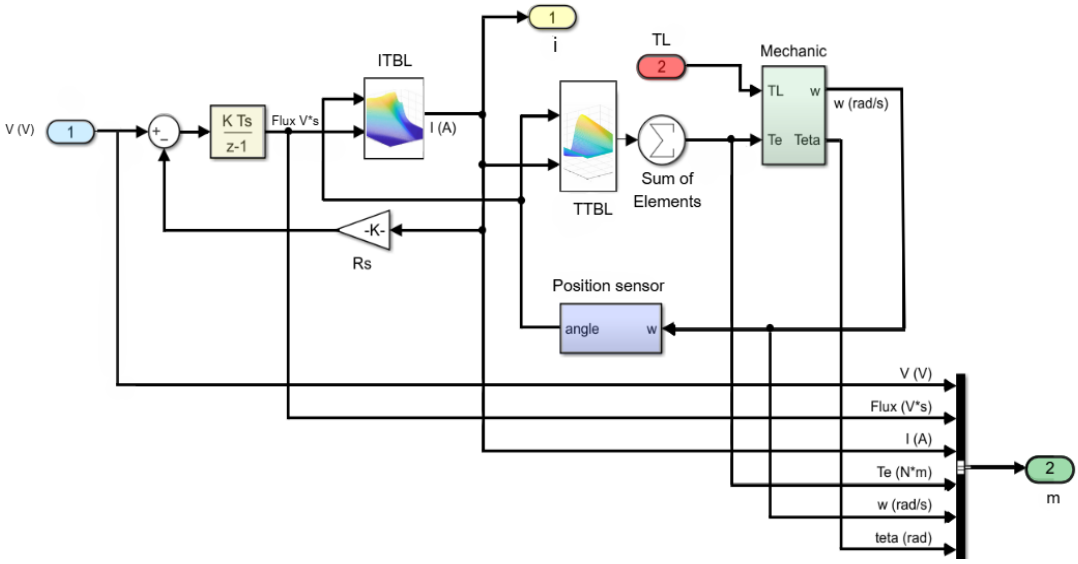

Figure 3.12: Simulink model of SRM

The MATLAB/Simulink model of the SRM consists of an electrical and mechanical model.

Input voltages are fed to the electrical model and measured by using a connector. The magnetic flux is calculated by integrating the voltage drop in the winding resistance and the input voltage difference. The controlled current source is used to inject the current produced by the non-linear current lookup table ITBL ($i(\psi, \theta)$) in the stator windings.
To compute the lookup tables ITBL and TTBL needed by the chosen model, a specific function is called prior to the simulation commencing. A specific model provided by the user FTBL lookup table uses the interpolation of cubic spline to create ITBL, while TTBL is acquired by numerical integration. The current lookup table is obtained using the analytical expression for the generic model.
The overall torque generated by the motor's acquired nonlinear function TTBL ($T_e(i, \theta)$) is used to calculate the electromagnetic torques generated by each stator winding. Those characteristics are obtained from the characteristics of magnetization required for modeling and can be achieved using either finite element method.

3.9 The 6/4 SRM Power Converter Topologies

SRM operation is relatively simple due to its ability to operate with unidirectional currents. In SRM drive the control is achieved by using a single switch. Whereas in AC motor drives minimum of two switches are required. Also, before undergoing regeneration the phase winding had to be de-magnetized [63] and a path had to be provided for de-magnetizing energy during commutation of the respective phase Moreover, the switch and phase winding are sequentially in the Motor drive but the series connection of switches with the phase winding is not possible in AC motor drives due to damage that may occur during the shoot-through faults.
In addition, the switched reluctance motor phases are independent and continuous uninterrupted operation is possible in the event of one winding failure [64].

3.9.1 Necessity of the power converter in SRM Drive

The power converter allows the SR motor to be powered from the DC source externally. It consists of a control loop for speed and torque. The signals from the controller are traced by the power converter, and based on those commands the motor phase gets energized and de-energized at suitable time intervals.
In addition to transferring energy, the power converter regulates the phase current to meet

the drive's precise specifications. To regulate the performance of the SRM, the outer speed loop consists of a rotor position sensor, which senses the encoder. Excitation of the phase winding of the motor at the area of increasing inductance is necessary for the motoring mode of operation.

The following requirements must be met when choosing a particular power converter:

- During increasing the inductance profile, the current energizes the winding
- During this energization, increased generated torque should be obtained, which is achieved by modifying the current
- During commutation, the stored magnetic energy has free-wheel through the load or feedback to the DC source.
- Quick de-magnetization capability

In this respect, many researchers have developed various power modulators including Asymmetric bridge converter, Resistive dump(R-dump), Capacitive dump(C-dump), R-dump with for demagnetization type, C-dump for de-magnetization type, series, and parallel type etc. But in this thesis work, an ASC is employed for its complete phase independence, very good performance, simple control efficiency, high fault tolerance, and less current ripple.

3.9.2 Asymmetric Bridge Converter

The Asymmetric bridge converter is a well-known configuration converter topology, which includes a pair of switches and diodes per phase to attain the unipolar switching scheme. Figure 3.13 presents the three-phase asymetric converter. Improving the noise and reducing the current ripple are the primary benefits of unipolar switching. The current control method is favored over the voltage control method in an ASB converter to properly regulate the phase current.

The constant current reference is used in the phase current control loop in the SRM, and the real phase current is contrasted with it. With a permitted current change Δi, an error is created and analyzed by the hysteresis controller; if the limits of error exceed the range, both switching gate are shut off at once. The current route is then taken to the DC supply by the freewheeling diodes.

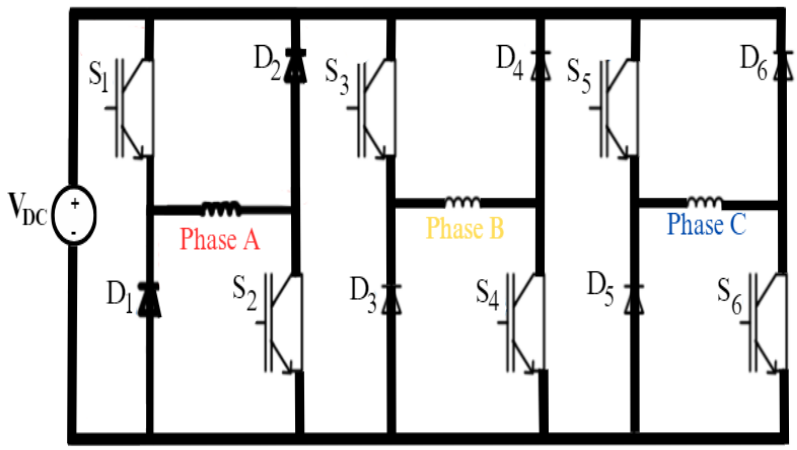

Figure 3.13: Three-phase AHB converter

Asymmetric H-bridge converters can be operated in three different modes:

- **Mode 1: Magnetization or Conduction Mode** consider phase A for operation, both S_1 and S_2 are ON switch status to energize Phase A. Consequently, the current passes through V_{dc} and make a loop with phase A and the two switches as shown in Figure 3.14-i. Consequentially, the current flow magnetizes the phases; this mode is called magnetization mode. The voltage across the energized phase is called the magnetization voltage, and it is equal to $+V_{dc}$.

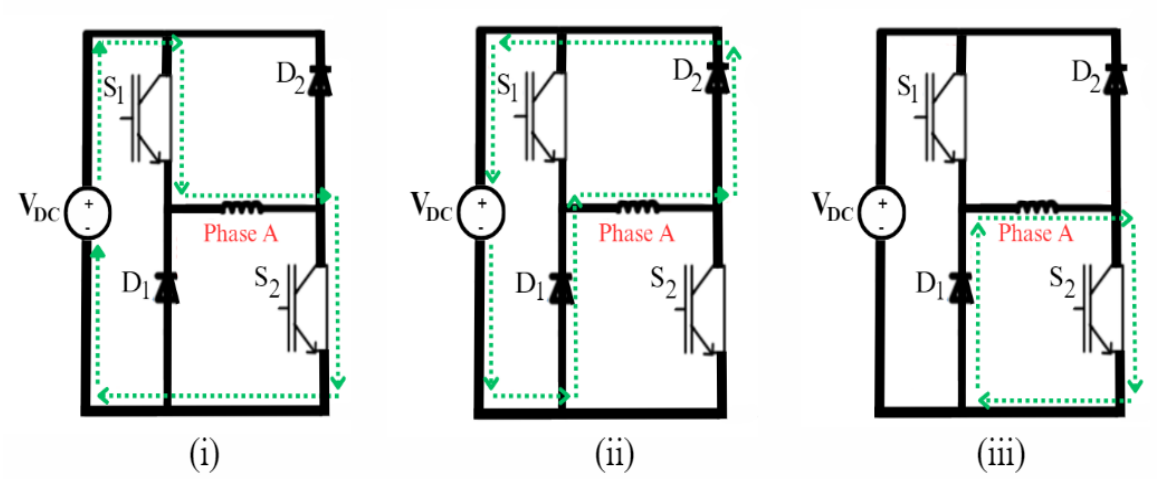

Figure 3.14 Operating modes of SRM with AHB converter

- **Mode 2: Demagnetization or Commutation Mode:** Figure 3.14-ii indicates the last mode of operation is called demagnetization mode, where both S_1 S_2 are turned OFF with forward bias D_1 D_2. In this mode, current passes through the D_2, phase A D_1, and supply. The voltage is equivalent to $-V_{dc}$. During demagnetization, the energy stored is returned to the origin, which can recharge the supply.

- **Mode 3: Freewheeling Mode** The switch S_1 is switched off when the current exceeds the reference phase current, which causes the diode D_2 to become forward-biased. The direction of phase current freewheels through phase A, S_2, and D_2. Figure 3.14-iii depicts the freewheeling mode and the voltage $V_{Dc} = 0$ due to no energy returned

3.10 Dynamic Analysis of Electric Vehicles

The drivetrain of a vehicle is an asset of Series parts that distribute power to the vehicle's driving wheels. An electric vehicle is generally perceived as simpler and comprises a battery acting as source of energy and the driving mechanism uses an electric motor.
Typical electric vehicle configurations are shown in Figure 3.15. As can be observed, the electric motor rotates creating torque to drive the gearbox and differential to supply power to the wheels. Speed reduction and associated torque multiplication are held by employing a single-speed gearbox.

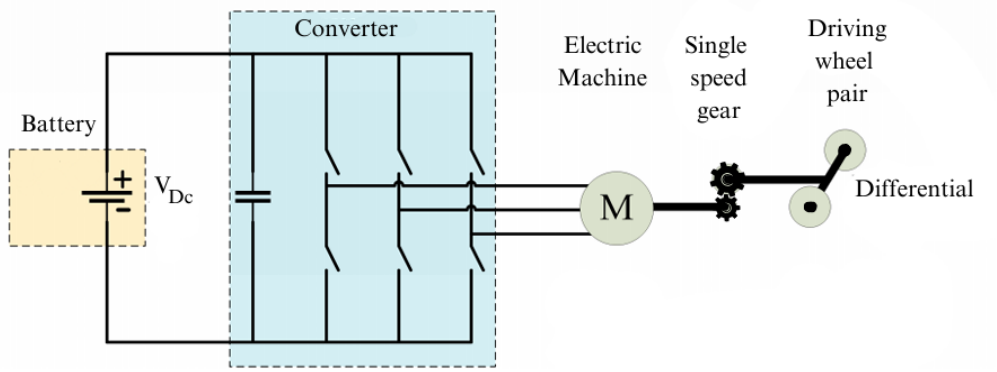

Figure 3.15 Electric vehicle drivetrain configuration [65]

A differential is required between the left and right traction wheels to allow them to rotate at slightly different speeds during turns. This enables the outside wheels to spin faster than the inside wheels, facilitating smoother turns. In an electric car, engaging the reverse gear can be easily achieved by altering the power phase sequence.
The tractive needs of the power train are ascertained according to a basic model of vehicle kinematics [66]. Various forces working against EV are represented by the model, as seen in Figure 3.16. They are primarily divided into four categories.

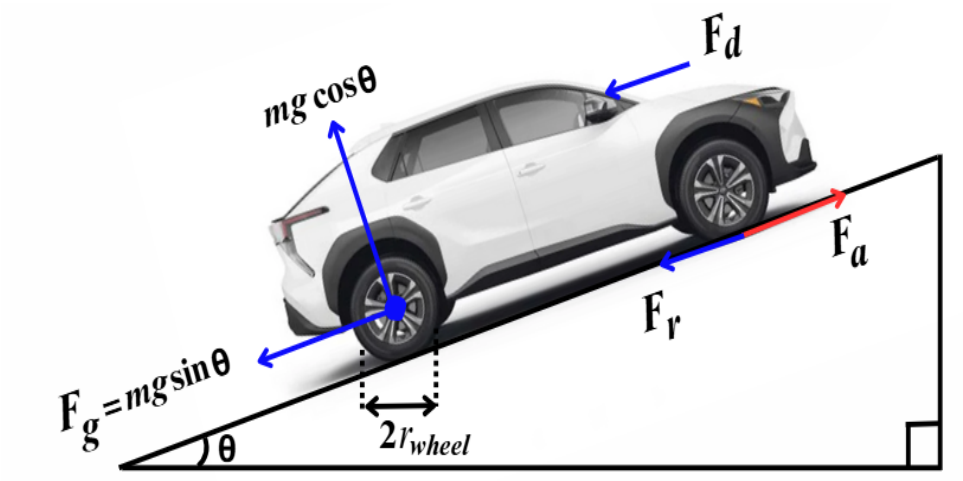

Figure 3.16 Forces appearing on the vehicle body, uphill movement

Selecting the appropriate power rating of the motor and other motor characteristics requires calculating the net force required to move the vehicle.

The force needed to overcome the resistive forces and to drive the wheel is called the resultant force. It is obtained as:

$$F_{res} = F_r + F_d + F_a + F_g \tag{3.22}$$

Where F_r, F_d, F_a, and F_g represent the rolling resistance, the air drags, the acceleration resistance, and the gradient resistance respectively.

3.10.1 Rolling Resistance Force

It prevents (opposes) tires from rolling. The friction between the EV tires and the pavement is the source of the force. Maintaining the highest feasible tire inflation will help to reduce this force [67]. Table 3.2 presents the specification parameters of EVs. The force of rolling resistance is obtained using:

$$F_r = K_r \cdot mg \cdot \cos(\theta) \tag{3.23}$$

$$F_{rr} = 0.01 \times 870\,\text{kg} \times 9.81\frac{\text{m}}{\text{s}^2} \times \cos(17^\circ) = 81.6\,\text{N}$$

Where K_r, m, g and θ are the rolling resistance coefficient, the gross vehicle mass in kg, the gravitational constant equal to 9.8 m/s^2, and the angle of elevation in degree respectively.

The power through required to overcome 81.6N resistive force:

$$P_r = F_r * V = 81.6\,\text{N} \times \frac{90,000\,\text{m}}{3600\,\text{s}} = 2.04\,\text{kW} \tag{3.24}$$

Table 3.2 Specification parameters of EVs

Parameter	**Symbol**	**Value**	**Unit**
Maximum Power	P	22	kW
Maximum vehicle speed	V	90	km/hr
Vehicle mass	M	870	kg
Frontal area	A_f	2.688	m^2
Radius of wheel	r	0.2764	m
Rolling coefficient	K_r	0.01	–
Aerodynamic coefficient	C_d	0.25	–
Aerodensity	ρ_a	1.2041	kg/m^3
Acceleration due to gravity	g	9.81	m/s^2
Efficiency of the transmission gear system	η	0.9	–
Gear ratio	i	6	–
Maximum gradient angle	θ	17	deg

3.10.2 Gradient Force

The resistance a vehicle experiences when ascending a hill or overpass or when moving down a slope is known as its gradient resistance (F_g) [68]. It is a pulling force required to overcome the resistance that an incline or decline in the road surface possesses. A moving vehicle on a slope experiences a gravitational force component, and this force either assists the vehicle in moving downhill or resists it in moving uphill.

The force due to the gradient was determined using Equation 3.25:

$$F_g = mg \cdot \sin(\theta) \tag{3.25}$$

with F_g being the gradient force in N, m being Gross of the vehicle mass in kg, g is gravitational acceleration in m/s^2 and θ being angle of elevation in degree.

$$F_g = 870\,\text{kg} \times 9.81\,\frac{\text{m}}{\text{s}^2} \times \sin(17^\circ) = 2495\,\text{N}$$

The power required to resist the gradient (pulling) force, assuming the vehicle climbs a 17-degree gradient at a speed of around 15-20km/hr, is:

$$P_g = F_g * V = 2495\,\mathrm{N} \times \frac{20,000\,\mathrm{m}}{3600\,\mathrm{s}} = 13.9\,\mathrm{kW}$$

3.10.3 Aerodynamic Drag Force

A force known as aerodynamic drag (F_d) opposes the motion of a vehicle moving through the air at a specific speed. The air in front of the vehicle compresses due to its movement, but it is unable to disperse right away, resulting in a high-pressure area. However, the air behind the car is unable to swiftly fill the space created by its speed, creating a low-pressure pocket.

A high-pressure zone at the front pushes against the vehicle's motion, while a low-pressure zone at the back drags it backwards. These two pressure zones are created while the vehicle moves. The friction between the airstream and the electric vehicle (EV) generates the aerodynamic force, which functions as a resistive force [69].

The aerodensity in ρ_a in kg/m^3, the vehicle's frontal area A_f in m^2, and velocity of the vehicle V may all be used to express it:

$$F_d = \frac{1}{2} \cdot \rho_a \cdot C_d \cdot A_f * (V + V_w)^2 \tag{3.26}$$

where V, V_w, C_d are the vehicle's velocity ($V = 0$ duetoinitial), velocity of the wind, and drag coefficient.

$$F_d = \frac{1}{2} \times 1.2041\,\frac{\mathrm{kg}}{\mathrm{m}^3} \times 0.25 \times 2.688\,\mathrm{m}^2 \times \left(23.6\,\frac{\mathrm{m}}{\mathrm{s}}\right)^2 = 225.3\,\mathrm{N} \tag{3.27}$$

and the overcome power is:

$$P_d = F_d * V = 77.9\,\mathrm{N} \times \frac{90,000\,\mathrm{m}}{3600\,\mathrm{s}} = 1.95\,\mathrm{kW} \tag{3.28}$$

Figure 3.17 illustrates that the aerodynamic force grows proportionally to the square of the car's speed. According to Equation 3.26, the drag force is directly related to the sum of the wind speed and the square of the car's speed. As the car's speed rises from 0 km/hr to 85 km/hr, the force increases from 0 to 77.9 N.

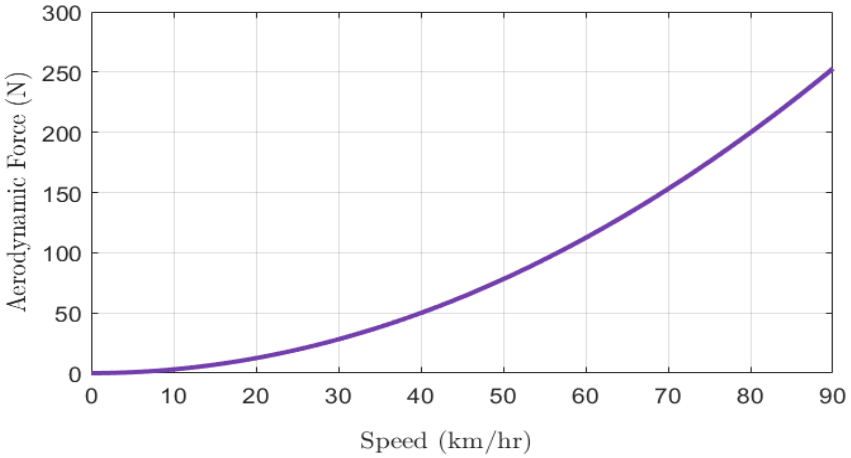

Figure 3.17 Aerodynamic drag force plotted against the car's speed in km/hr

3.10.4 Acceleration Force

Newton's second law determines the acceleration force (F_a), which allows the vehicle to go from a motionless position to a specified speed in a certain amount of time. The rolling resistance, gradient force, and aerodynamic drag are the main forces affecting the vehicle when it is traveling at a constant speed.

Acceleration force, which is required for the electric vehicle to accelerate or decelerate, may be represented as follows using Newton's second law: [70]:

$$F_a = m\frac{dv}{dt} \tag{3.29}$$

F_a represents acceleration force, m denotes the mass of the vehicle, and v is the vehicle speed.

When designing vehicle dynamics, additional forces must also be taken into account, such as the equivalent inertial force during acceleration (which includes both linear and rotational inertias caused by the vehicle's mass and rotating parts like the gear train and wheels), aerodynamic lift force, wheel force, and others. Typically, these forces are relatively small compared to the primary forces previously mentioned and are estimated to contribute no more than 1.5 kW. As a result, the total tractive power needed to propel the vehicle is the combined sum of all these power components.

$$P_T = (2.094 + 13.9 + 1.9 + 1.5)\,\text{kW} = 19.34\,\text{kW}$$

It is not appropriate to choose an electric motor with an output power rating of 19.34 kW. The power losses that take place when power is transferred to the wheels must be taken into consideration. Therefore, the following formula is used to calculate the necessary mechanical power output to move the vehicle:

$$P_{driving} = \frac{P_{max}}{\eta_{\text{transmission}}} = \frac{19.34\,\text{kW}}{0.9} = 22\,\text{kW}$$

and the power in HP:

$$P_{driving(\text{hp})} = \frac{P_d}{745.699872} = \frac{22\,\text{kW}}{745.699872} = 140\,\text{hp}$$

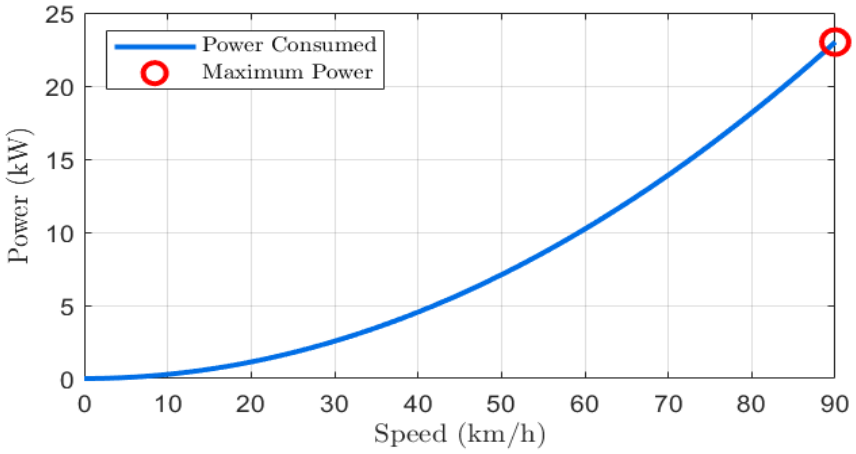

Figure 3.18 Power consumed versus Speed of the vehicle (km/hr)

Thus, the required $P_{driving}$ used to select the motor. Because the road gradient angle θ is 0 while a vehicle is traveling on a level road, its sine value is zero, and so the gradient force is zero. Rolling resistance, aerodynamic drag, and acceleration force are the only factors affecting the vehicle as a result. Given a fully loaded vehicle accelerating at 1.8 m/s^2 on a level road in Figure 3.18, the power required to resist these pressures is 22 kW, which is less than the maximum power that was predicted. The car can accelerate from rest to its maximum speed in 13 seconds with this configuration.

Based on the calculated total applied force and power requirements, the motor specifications are described in Table 3.2.

3.11 Battery Sizing

The battery is a core component of an electric vehicle, which serves as the main source of energy. To ensure that crucial and the design should satisfies the energy demands of the vehicle.The common battery technologies seen in electric vehicles to date are lithium-ion (Li-ion), nickel metal hydride, nickel cadmium, and lead acid. batteries [71]. Because of its high running voltage levels, high power density, broad variety operating temperature, long maintenance life, reduced self-discharge rate, and absence of memory influence, Li-ion battery technology is regarded as outstanding to all different battery technologies [72].

The battery capacity, quantified in kilowatt-hours, defines the energy available for driving.

Table 3.3 Parameters for calculation of battery sizing

SPECIFICATIONS	**VALUE**
Li-ion cell	
Rated voltage	3.7V
Capacity	2500mAh
Charging voltage	4.2V
Weight/cell	45g
Energy density	9.13Wh
Motor	
Nominal voltage	240V
Power	22kW
Vehicle	
Maximum speed	90km/hr
Expected range of travel	150km

To calculate the required battery pack rating for the chosen 22 kW traction motor and select the lithium-ion battery with parameters from Table 3.3. given the motor's required voltage of 240V, we must determine the battery size needed to power the motor at the fastest speed the car can reach at 90 km/h with an expected range of 150 km.

The current drawn by the traction motor at different operating conditions or peak current demand can be calculated as:

$$\text{Current demand} = \frac{\text{power}}{\text{voltage}} = \frac{22\,\text{kW}}{240\,\text{V}} = 91.6\,\text{A}$$

Battery cell capacity energy is typically expressed in Wh, which tells the amount of energy that a battery cell can store is determined by:

$$\text{Battery Power} = \text{Battery cell capacity} \times \text{Battery cell voltage} \tag{3.30}$$

$$\text{Battery power} = 2.5 \times 3.6 = 9Wh$$

Wh/Kg, a measure of battery cell energy density, indicates how much energy is stored per single unit weight. fore More energy with a smaller weight is indicated by a higher energy density. It is computed as follows:

$$\begin{aligned} \text{Energy density} &= \frac{\text{Cell energy}}{\text{Cell mass}} \\ &= \frac{9\,\text{Wh}}{0.045\,\text{kg}} = 200\,\text{Wh/kg} \end{aligned} \tag{3.29}$$

The total stored energy within a battery pack is determined by:

$$\begin{aligned} \text{Total energy of the Battery pack} &= \text{supply voltage} * \frac{\text{current drawn}}{\text{vehicle speed}} * \text{distance} \\ &= 240\,\text{V} \times \frac{91.6\,\text{A}}{90\,\text{km/hr}} \times 150\,\text{km} = 37\,\text{kWh} \end{aligned} \tag{3.30}$$

The overall connected series cell voltage in a battery pack is the sum of individual cells, while the capacity (in Ah) remains the same.

$$\text{Number of cells in series} = \frac{240\,\text{V}}{3.7\,\text{V/cell}} = 65\,\text{cells} \tag{3.31}$$

In a battery pack, a string refers to multiple cells connected in series. The string of energy content is the product of the total voltage of the string and capacity. Here's the formula for that:

$$\begin{aligned} \text{The string content of energy} &= \text{Number of cells in series} \times \text{battery cell Energy} \\ &= 65 \times 9 = 585\,\text{Wh} \end{aligned} \tag{3.32}$$

To find the number of strings in a battery pack, the cells are arranged in series the total energy of the battery pack divided by each string's content of energy.

$$\begin{aligned} \text{Number of strings in battery pack} &= \frac{\text{battery pack total energy}}{\text{Energy content of each string}} \\ &= \frac{37\,\text{kWh}}{585\,\text{Wh}} = 63.24 \approx 64\,\text{strings (Approx.)} \end{aligned} \tag{3.33}$$

Ampere-hours (Ah) is the unit for Battery pack capacity and can be calculated by determining the total energy battery pack with its cell capacity

$$\begin{aligned} \text{Battery pack capacity} &= 64 \times 2.5 \\ &= 160\,\text{Ah} \end{aligned} \tag{3.34}$$

And, the number of total cells in a pack is the product of cells and string :

$$\begin{aligned} \text{Total number of cells} &= 64 \times 65 \\ &= 4160\,\text{cells} \end{aligned}$$

The battery pack total is computed by summing the total masses of individual cell:

$$\begin{aligned} \text{Battery pack mass} &= 4160 \times 0.045\,\text{kg} \\ &\approx 188\,\text{kg (Approx.)} \end{aligned}$$

Each cell's peak current in the configuration of parallel results in battery pack:

$$\begin{aligned} \text{Peak current} &= (\text{crate} \times \text{Cell capacity}) \\ &= 2 \times 2.5\,\text{Ah} \\ &= 5\,\text{A} \end{aligned} \tag{3.35}$$

The peak current of the pack determined:

$$\begin{aligned} \text{Peak current of the pack} &= \text{peak current} \times \text{Number of strings} \\ &= 5 \times 64\,\text{strings} \\ &= 320\,\text{A} \end{aligned} \tag{3.36}$$

The peak power delivered by the battery pack can be calculated by 3.37

$$\begin{aligned} \text{peak power} &= \text{peak current} \times \text{Voltage} \\ &= 320\,\text{A} \times 240\,\text{V} \\ &= 76.8\,\text{kW} \end{aligned} \tag{3.37}$$

Chapter 4

Controller Design

4.1 Chapter Overview

This chapter covers the detail design, the basic structure, and thorough explanations of fuzzy logic controllers (FLC). It also covers the speed controller design for switched reluctance motors, presenting each step of the algorithms involved. Furthermore, it elucidates the principles of DTC, detailing the acquisition of of components, including voltage voltage space vectors, switching table design, and sector determination.

4.2 Fuzzy logic controller

An intelligent computational method for complicated and nonlinear framework systems that offers a robust structure and simple solution. It doesn't require precise knowledge of a mathematical model. It uses basic measurement to represent an ambiguity languages such as artificially or naturally to meaningfully. The theory of the Fuzzy set employs linguistic values to express vague concepts. Randomness characterizes the uncertainty of an event's occurrence, while fuzziness describes its ambiguous nature.

Fuzzy logic control is established on fuzzy sets, which are described by their unclear and imprecise outlook, abstract concepts, and absence of unambiguous boundaries. Every element inside a fuzzy set relates to a certain degree, as determined by the membership function. This membership function translates crisp inputs into a normalized or fuzzy domain, with characteristic function values ranging between 0 and 1.

A fuzzy set is a direct extension of a classical set, mathematically defined by assigning each element in a universe of discourse a membership value ranging from -1 to 1 through mem-

bership functions. It consists of a collection of IF-THEN rules that make uncertain and vague predictions using fuzzy reasoning models, such as the Sugeno (or TSK) and Mamdani models. Sugeno-type systems can model any inference system with linear or constant output membership functions, whereas the Mamdani model generates either linear or nonlinear outputs.

The capacity of fuzzy logic systems to make wise judgments and execute suitable control actions to integrate expert knowledge into the system architecture to effectively manage ambiguous, partial, and indistinct information has attracted a lot of attention.

A fuzzy logic controller uses experience, intuition, and reasoning instead of relying solely on mathematical models. It produces output based on input values as human-like thinking and eliminates control issues in systems. FLC is a distinct technique for managing uncertain and imprecise nonlinear systems [73].

4.2.1 FLC's fundamental structure

The classical set characteristics function assigns either a binary set for every element within universal set, indicating whether they belong within crisp set being considered. Different levels of membership within the set members handled within the fuzzy set. Experience and problem specificity are the keys to determining the membership function. Different kinds of membership functions are frequently employed in fuzzy set theory for step of converting crisp input toward fuzzy inputs.

Figure 4.1 illustrates the four steps of the fuzzy logic controller: Fuzzification of the input values, rule Base, fuzzy expert engine, and Defuzzification.

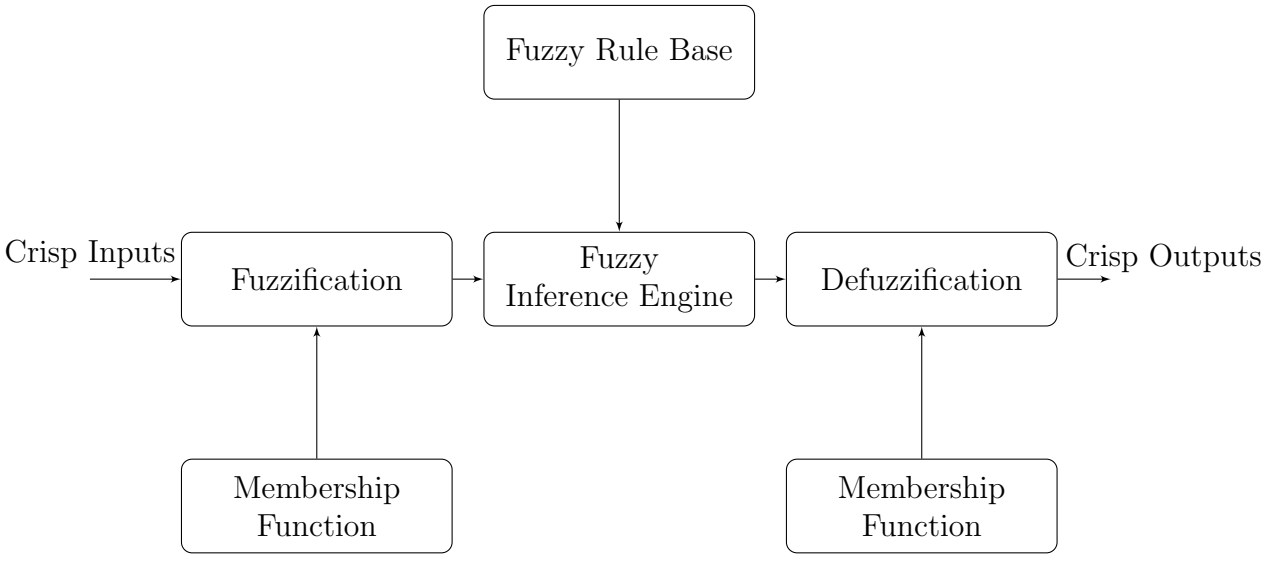

Figure 4.1 Basic Parts of Fuzzy Logic Control

i. **Fuzzification**

The initial step in designing a fuzzy logic controller and includes transforming a precise or real value into a fuzzy variable. Crisp input values are translated into linguistic variables. Impreciseness, vagueness, and ambiguity of the real-life is the occurrence of uncertainty. A membership function is a useful tool for expressing this ambiguity.

ii. **Fuzzy rule base** It is the core part of the controller. All the necessary stores information to regulate the system, and it is derived from the skilled operator. As a result, it is regarded as the core component of the controller as it enables the controller to independently make wise judgments and use the fuzzy rule base to determine the appropriate control actions.

The two components of the fuzzy rule are IF (antecedent)-THEN (consequent), where the IF section establishes the condition and the appropriate corrective control action is explored in the consequent part. The quantity of input, output, and membership functions associated with each variable determines how many rules are in a rule base.

iii. **Fuzzy Inference Engine** An essential component of a fuzzy logic system, it generates output decisions or outcomes by using fuzzy rules to examine input data. Among fuzzy inference models, the Mamdani inference is the most popular. The process of inference involving aggregation, implication, and accumulation results in the development of a fuzzy multiplier the output determined by the logical rules. Therefore, the inference model generates an outputs for every rules that is activated.

Multiple rules in the fuzzy rule base will be activated as the process's crisp measurement (input) will be a component of multiple membership functions (fuzzy set). Next, the inference engine determines the appropriate control actions by utilizing the provided fuzzy rule base.

$$\mu_{FRi}(p,q,r) = t(\mu_{pl}(p),\ \mu_{ql}(q)) \wedge \mu_{rl}(r) \tag{4.1}$$

$$= (\mu_{pl}(p) \Lambda \mu_{ql}(q)) \Lambda \mu_{rl}(r)$$

Where, FR_i express the i^{th} the rule base for fuzzy rule, which has n rules, T-norm operator(t) used for the normalization for fuzzy output for i^{th} rule inference system. The implication of mamdani fuzzy rule antecedent section is computed using T-norm operator.

iv. **Defuzzification** The fuzzy inference engine's fuzzy output needs to be Transformed into output of crisp for supervision and system control. Defuzzification is the procedure that converts the controller's inaccurate output into a clear value. The center of gravity is the defuzzification technique frequently employed. With u_i standing for the output center MF and $(\Delta e, e)$ as the value of crisp output regarded as the minimal value, the crisp output is provided by:

$$u(\Delta e, e) = \frac{\sum_i^n u_i \min(\mu_{xl}(\Delta e), \mu_{yl}(y))}{\sum_i^n \min(\mu_{xl}(\Delta e), \mu_{yl}(y))} \tag{4.2}$$

4.3 Speed controller design of SRM using FLC

FLC is used for developing control algorithms in various applications of nonlinear, uncertain, and imprecise characteristics. It provides better results than conventional control methods by the general methodology of fuzzy of set, where the MF is in the range of 0-1, making it feasible to construct processing systems.

Controlling the speed of SRM is difficult due to its nonlinear characteristics. However, the fuzzy controller is made to effectively regulate and sustain speed. Figure 4.2 shows that the fuzzy controller system utilizes the crisp input variables are error speed signal (E) and change of rate speed error (CE). reference current (I_{ref}) is the defuzzification crisp output. Speed error and rate of change speed error variables are described as follows:

$$\begin{aligned} E(k) &= \omega_{ref}(k) - \omega(k) \\ CE(k) &= E(k) - E(k-1) \end{aligned} \tag{4.3}$$

Where ω_{ref}, $\omega\,(k)$, $E\,(k)$, and $CE\,(k)$ are the reference speed, actual speed, speed error, and error of change rate respectively.

Step 1: Fuzzification of the input variables

Fuzzification is the initial phase of converting the crisp inputs into linguistic variables by using the Membership function and their ranges. The input linguistic variable represents the error of speed amount and the change of error signal. Seven linguistic variables are selected for every input fuzzy set: NL, NM, NS, ZE, PS, PM, and PL are Negative Large, Negative Medium, Negative Small, Positive Small, Positive Medium, and Positive Large along with their MF are depicted in Figures 4.3a and 4.3b.

Similarly, the o/p fuzzy set has seven specified variables, as shown in Figure 3.4c.

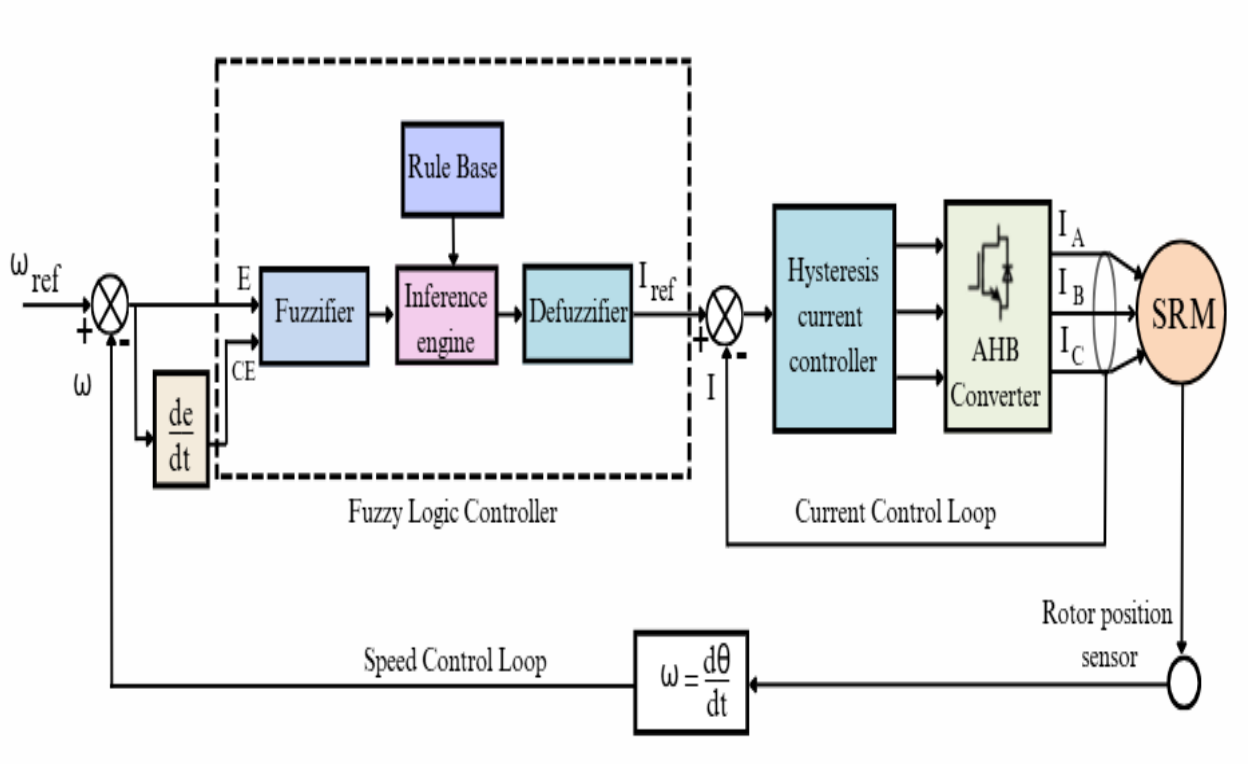

Figure 4.2 Block diagram of a speed control of SRM using FLC

Using a surface viewer, the output variable's dependence on the variables of the input is assessed.

Step 2: Design Rule base

Following the fuzzification of variables for inputs and outputs, the base of fuzzy rules is established according to Table 4.1. Mamdani fis is employed due to its intuitive nature and it allows the description of the expertise in a human-like manner. Also, its characters are highly accurate. According to the rule tables and 49 (7×7) IF-Then rules are determined based on choosing the proper reference torque, two inputs are needed: error of speed and change of speed as illustrated in Appendix B.2.

Step 3: Defuzzification

In the defuzzification process, the resulting fuzzy values are converted to numerical values (crisp o/p). The variables in the output are represented by constants with a digitalized name of [-1 1] which are interpreted as a negative large - positive large. Output Variables for defuzzification are chosen according to the rule base. In this procedure, the centroid-type defuzzification technique is applied.

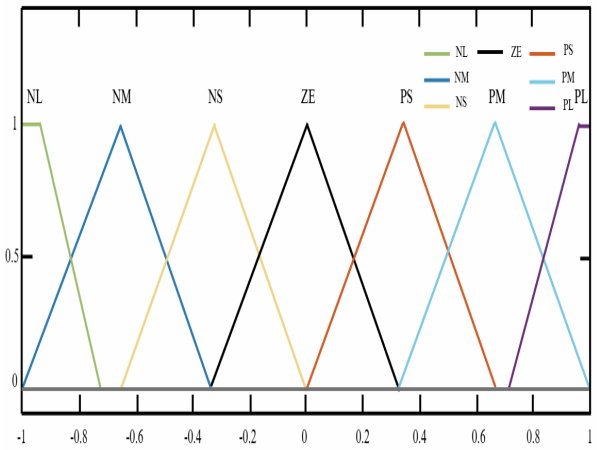

(a)

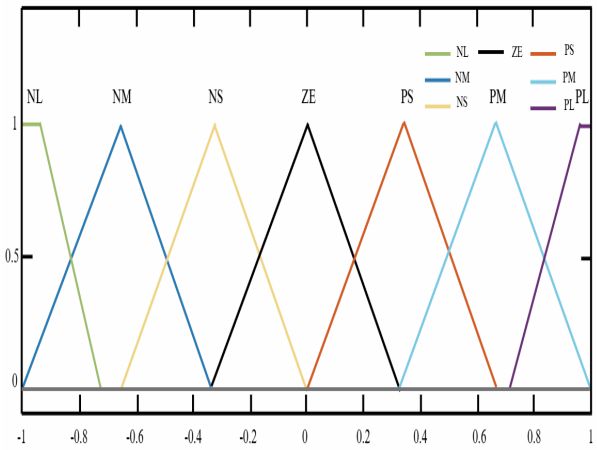

(b)

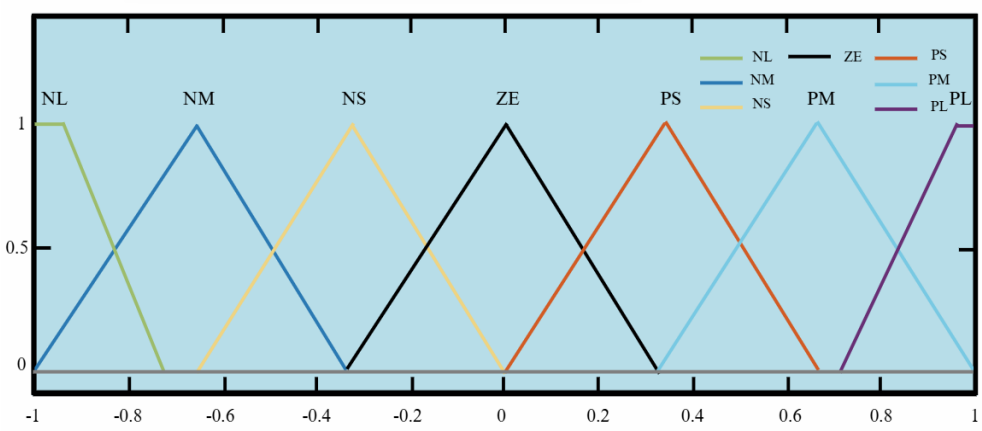

(c)

Figure 4.3 MF for (a) Error input speed, (b) Change error input speed (c) Output current reference

Table 4.1 Fuzzy rule base matrix

Error	**Change error**						
	NL	**NM**	**NS**	**ZE**	**PS**	**PM**	**PL**
NL	NL	NL	NL	NL	NM	NS	ZE
NM	NL	NL	NL	NM	NS	ZE	PS
NS	NL	NL	NM	NS	ZE	PS	PM
ZE	NL	NM	NS	ZE	PS	PM	PL
PS	NM	NS	ZE	PS	PM	PL	PL
PM	NS	ZE	PS	PM	PL	PL	PL
PL	ZE	PS	PM	PL	PL	PL	PL

4.4 Direct Torque Control (DTC) and its Principle

SRM has intrinsic simplicity in structure and less price. Due to its doubly salient structure, magnetic saturation, and reluctance variation, it has inherent torque ripple in its output torque. The control of this drive is difficult if the torque ripple is not reduced.
DTC has certain good features such as a simple algorithm, it does not require bidirectional current, knowledge of motor parameters, and a set of motor equations. In addition to this, it successfully removes the torque ripple in output torque characteristics by controlling the motor torque and flux with a hysteresis controller. DTC computes torque and flux in the stator coordinate using a space of voltage vector. [74].

4.4.1 Fundamental concepts of direct torque control in SRMs

In SRM, torque generation relies on the principle of reluctance. Because of the nonlinear behavior of magnetic saturation, its instantaneous torque is expressed as :

$$T(\theta, i) = \frac{\partial \lambda(\theta, i)}{\partial \theta} i \tag{4.4}$$

Whereλ, i, and θ are flux linkage, phase current, and rotor angular position respectively.
Unipolar drives are commonly used in SRMs, resulting in a consistently positive current flow in each motor phase. From expression Equation 4.4 the torque is directly linked to the variation of $\partial\lambda/\partial\theta$ exceeding zero, and the generation torque also be $T(\theta, i)$ positive.
When a flux vector is improved with the movement of in the same direction of rotor position, a variation positive torque is generated. In the delayed flux vector with θ, a negative torque is produced, for the movement in opposing direction.
The flux variation in negative and positive with the θ is termed as the deceleration and acceleration of flux. As a result in a novel of DTC Approach there are two principles [75]:

i. The motor maintains a constant amplitude for its stator vector flux linkage.

ii. Torque controlling is maintained in decelerating and Accelerating the flux vector.

The modified voltage equation in single-phase is expressed as:

$$\vec{\lambda_s} = \int_0^t (\vec{V_s} - R_s \vec{i_s})\, dt + \vec{\lambda_0} \tag{4.5}$$

Where $\vec{\lambda_0}$ and $\vec{i_s}$ are the initial phase flux vector and the current vector of stator respectively. In most cases, the resistance is little. Considering that the initial flux is always zero ($\vec{\lambda_0} = 0$) when the motor is started, and due to small resistance in the resistor the voltage dropped is ignored; in the small time of interval, Equation 4.5 stated as:

$$\Delta\lambda_s(\theta, i) = \vec{V_s}\Delta t \tag{4.6}$$

Notably, Equation 4.6 shows that the stator flux vector's variation is proportional with the voltage's amplitude and the time variation product and demonstrates how the stator flux vector varies in the same direction as the space voltage vector when applied to a single phase. As revealed by Figure 4.4 DTC of SRM comprises flux comparators, a switching table, hysteresis-based torque, and flux-linkage vector position data to produce voltage vectors of optimal for regulating the magnitude of electromagnetic torque and stator flux linkage.

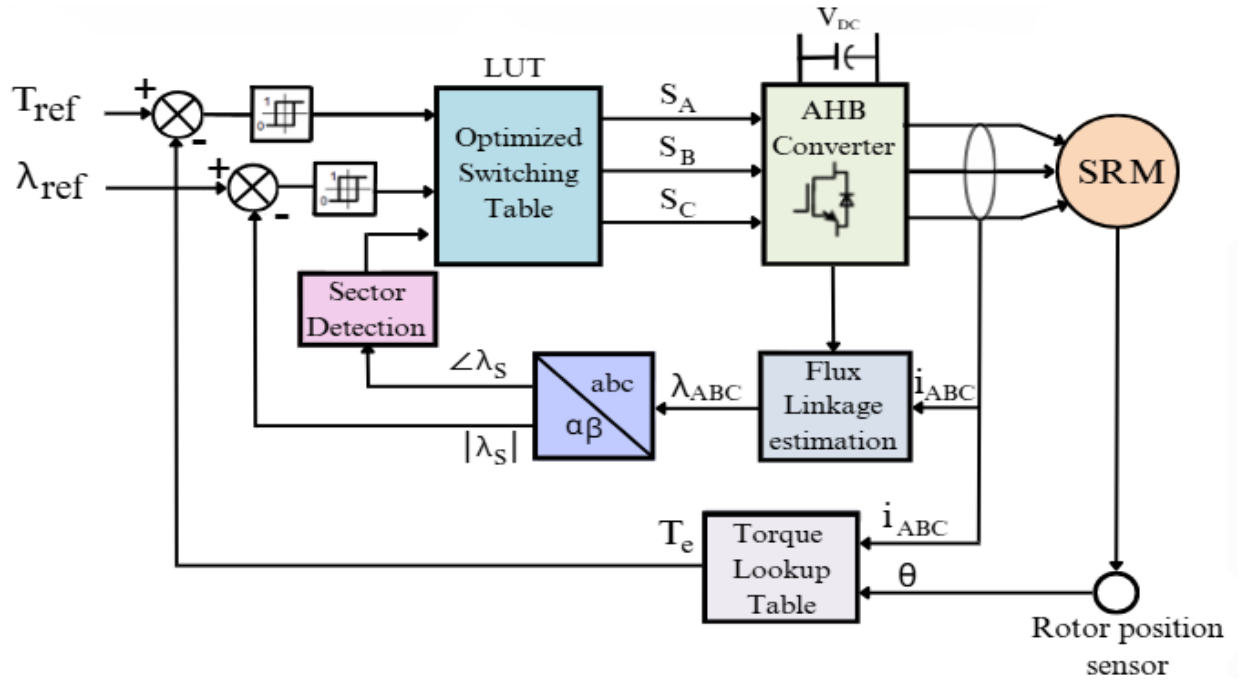

Figure 4.4 Basic elements of DTC in the SRM

4.4.2 Voltage vectors and Switching table of 3-phase

A power converter's switch can be in one of three states while it is operating. This is represented by the symbol '1,' and a positive voltage is provided to the winding when both switches are turned on. When one switch is in the "0" position during the freewheeling stage, no voltage is supplied to the winding. A negative voltage is provided to the winding when both power switches in the stator phases are off, which is represented by the voltage state of '-1'. Figure 4.5 displays the equivalent switching states of a single-phase winding, where S stands for the switching state. The switching table may be created as indicated in Table 4.2 by looking at the vectors and using the two DTC concepts.

Three different states of voltage are applied in every SRM phase. Hence, the setup of the state voltage vector (V_n) consists of one row and three columns in its structure as $V_n = (V_A, V_B, V_c)$, where V_A, V_B, and V_c are states of voltages applied to phase A, B, and C Correspondingly. For three-phase SRM, 120° spaces equally phases, and three axels are achieved over the concentric axels of the phases during tracing. As reflected in Figure 4.5 each phase is sectioned into positive and negative parts, located at the axel portion and the half of the other axel respectively.

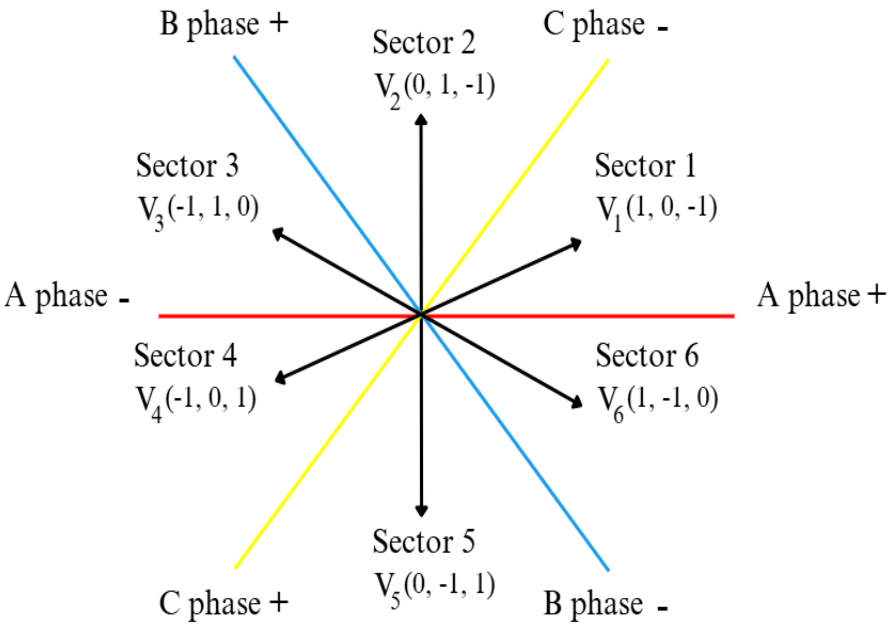

Figure 4.5 Definition of voltage space vector for 3-phase SRM

V_A, V_B, and V_C SRM vectors belong define the positive three-phase voltage vector of the windings state is 1, Similar to -1 state indicates the $-V_A$, $-V_B$, $-V_C$ voltage vector. For state 0, the voltage vector is zero

The AHB converter has $3^3 = 27$ possible switching state combinations. In the DTC algorithm applied to a three-phase SRM, only six voltage vectors with equal magnitude are defined separated by $\pi/3$ radians (60 deg). They are the fundamental voltage vectors and are located in the middle of the six zones as depicted in Figure 4.5.

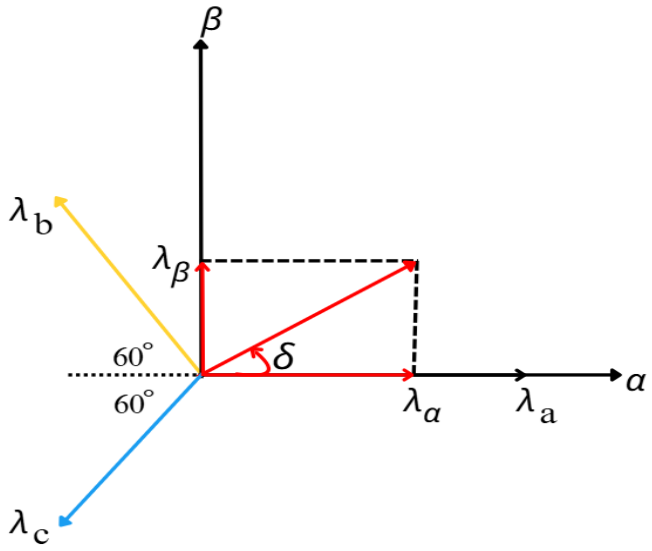

Figure 4.6 Clarke transformation of three-phase voltage

Individual phase flux linkage magnitude changes with time, but the direction stays constant along the stator pole axis. In order to resolve these vectors, the three-phase SRM's phase flux components are transformed into a stationary two-axis$\alpha - \beta$ reference frame. As shown in Figure 4.6, the flux vector may be computed by projecting the flux vectors onto orthogonal stationary frame.

Clarke transform is used to transform the particular three-phase SRM flux (λ_a, λ_b and λ_c) into a flux vector of two-frame orthogonal α - β (λ_α, λ_β) stator flux as:

$$\begin{aligned} \lambda_\alpha &= \lambda_a - \lambda_b \cos 60^\circ + \lambda_c \cos 60^\circ \\ \lambda_\beta &= \lambda_b \sin 60^\circ - \lambda_c \sin 60^\circ \end{aligned} \tag{4.7}$$

The two-axis orthogonal flux vector of the stator magnitude of the equivalent flux vector ($|\lambda_s|$) and angle of the rotor (δ) Which are outlined as:

$$\begin{aligned} \lambda_s &= \left(\lambda_\alpha^2 + \lambda_\beta^2\right)^{\frac{1}{2}} \\ \delta &= \arctan\left(\frac{\lambda_\beta}{\lambda_\alpha}\right) \end{aligned} \tag{4.8}$$

Assume the stator's flux vector are Placed in the S^{th} sectors (S= 1, 2, 3, 4, 5, and 6). Voltage vector selection is determined jointly with the sector and by the adjustment torque and flux linkage direction. To raise the stator flux's amplitude, the voltage vector's V_S, V_{S+1}, V_{S-1} can be employed, and V_{S+2}, V_{S+3}, V_{S-2} are applied for decreasing the flux's. So, the stator flux's when enhanced by V_{S+1} and V_{S-1} and reduced by V_{S+2} and V_{S-2} affects the torque's. Since V_{S+1}, V_{S+2} vectors move the stator flux linkages in the rotational direction and they contribute to raise within torque. However $V_{S-1}$and V_{S-2} decrease both the flux's against the opposite direction and the torque.

As a result, the switching tables are set up as shown in Table 4.2. V_0 and v_7 are null vectors which does not affect the flux, but voltage vectors V_1, V_2, V_3, V_4, V_5, and V_6 are the active voltage vectors applied to the optimal switching table.

Table 4.2 General Table Selection of DTC

Voltage vector	**Increase**	**Decrease**
Stator flux	V_{s+1}, V_{s-1}	V_{s+2}, V_{s-2}
Torque	V_{s+1}, V_{s+2}	V_{s-1}, V_{s-2}

Table 4.3 The designed Switching Table

Hysteresis error		**Sectors**					
		S_1	S_2	S_3	S_4	S_5	S_6
$H_\psi = 1$	$H_{T_e} = 1$	V_2	V_3	V_4	V_5	V_6	V_1
	$H_{T_e} = 0$	V_7	V_0	V_7	V_0	V_7	V_0
	$H_{T_e} = -1$	V_6	V_1	V_2	V_3	V_4	V_5
$H_\psi = 0$	$H_{T_e} = 1$	V_3	V_4	V_5	V_6	V_1	V_2
	$H_{T_e} = 0$	V_0	V_7	V_0	V_7	V_0	V_4
	$H_{T_e} = -1$	V_5	V_6	V_1	V_2	V_3	V_4

Chapter 5

RESULTS AND DISCUSSIONS

5.1 Chapter Overview

The present chapter explores and investigates the overall Simulink model of a fuzzy logic controller speed control-DTC-based system, analyzing and contrasting its simulation outcomes under various circumstances. MATLAB R2021a Simulink software models, tests, and verifies the study. In this chapter, a comparative analysis of results is performed regarding the proposed PI, Fuzzy, and FLC with DTC. Designed controllers with specified parameters are discussed with Performance comparison, load variation, parameter variation, and different reference speed tracing are performed.

5.2 Simulation Model for System Drive

The overall system model built in MATLAB Simulink model comprises control loops of torque and speed as outlined in Figure 5.1. The parameters used in the simulation are detailed in Appendix A.

To enhance system performance, two loops are performed in the designed system. The external loop consists of a speed controller for comparison of reference speed with the motor response, and its generated error is fed to FLC block. The speed controller output control is provided to the torque comparator by acting with motor torque.

The flux estimator, the two and three-level comparator, the sector selector, and the optimal switching table are installed in the inner loop of the system to regulate the output torque. After comparing the intended flux and torque values with the actual measured values, the switching table receives this control signal produced by hysteresis flux and torque control, which identifies the proper switching state. The calculated flux angle defines the region in which the flux vector is energized, and the output signal corresponds to the input provided to the switching table.

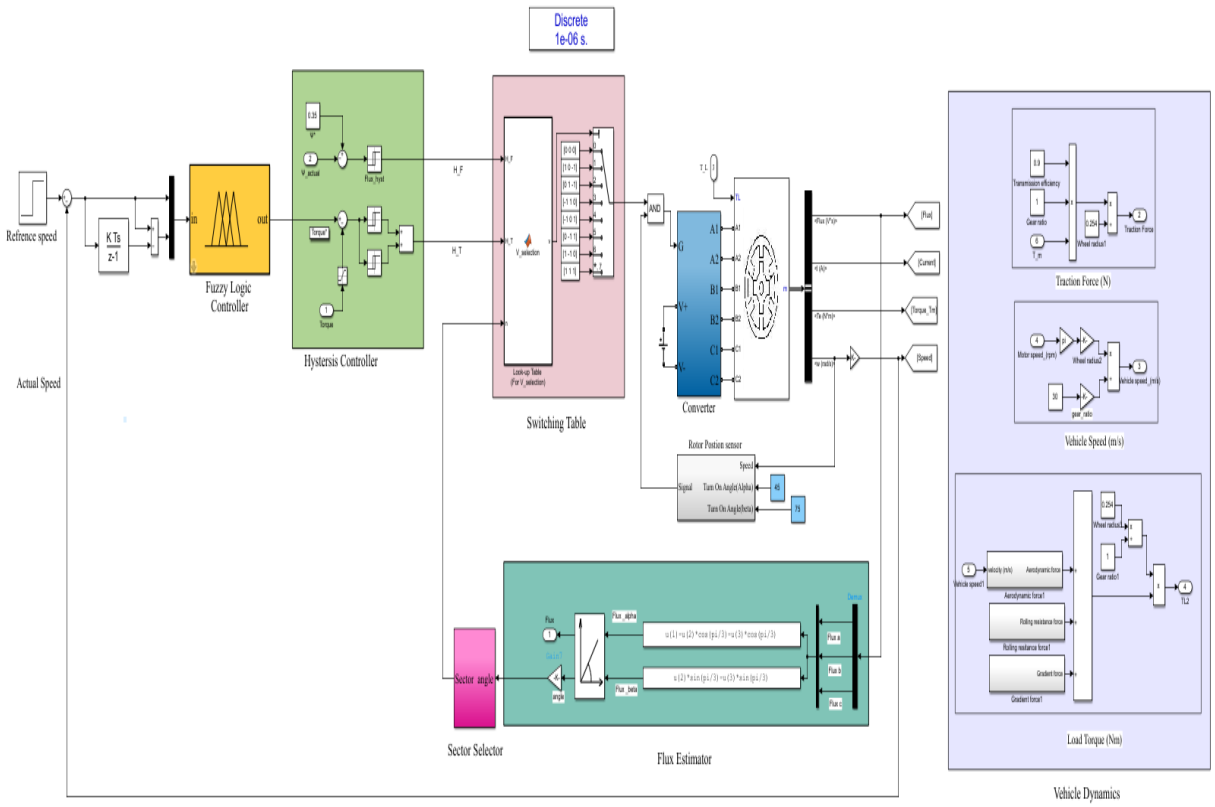

Figure 5.1 Block diagram of the overall system

In the simulation test conducted for this thesis, the motor's reference flux is maintained at a fixed value of 0.35 Wb. The flux and torque controller band limits are set to ±0.486 Wb and ±0.001 Nm, respectively. During the test, the motor operates at a constant speed of 2000 rpm.

5.3 Analysis of System without Controller

During the absence of a speed controller, the motor operates in open-loop modes. Flux variation observed from Figure 5.2 due to quick rapid excitation of the motor during the period (1 to 1.025 sec). Speed response of the system is displayed in Figure 5.3, it exhibits a high overshoot. The desired values attained at 0.18 sec and the system overshoot is more than doubled the reference speed, which is extremely high. When there is no control over the speed at the prespecified load, the motor operate at a higher speed due to a rapid phase excitation from the AHB converter resulting in producing a low reluctance in the instantaneous period because of the system's simple configuration. The speed of the vehicle with the prespecified load is depicted in Figure 5.4

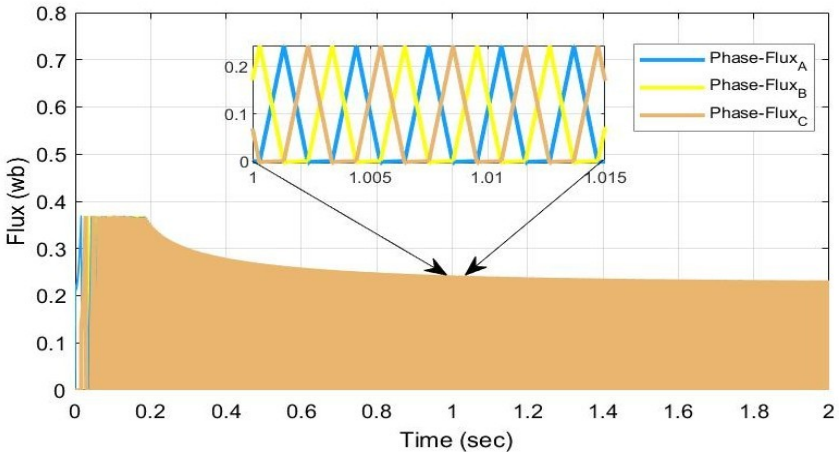

Figure 5.2 Phase Flux of the Motor

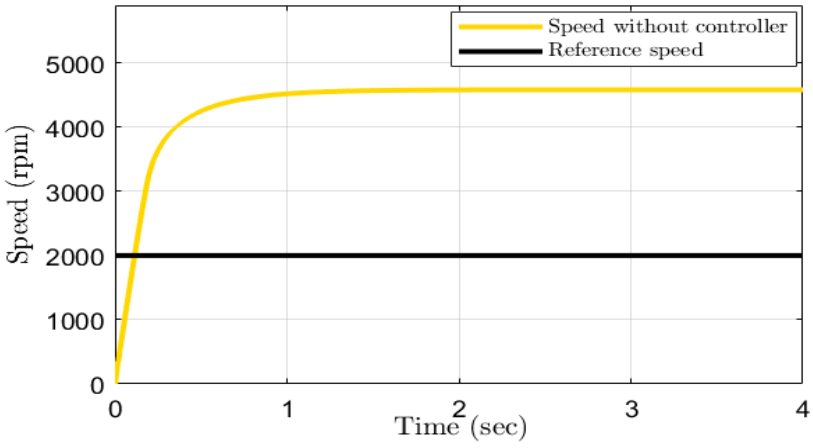

Figure 5.3 Speed response without a controller at no-load conditions

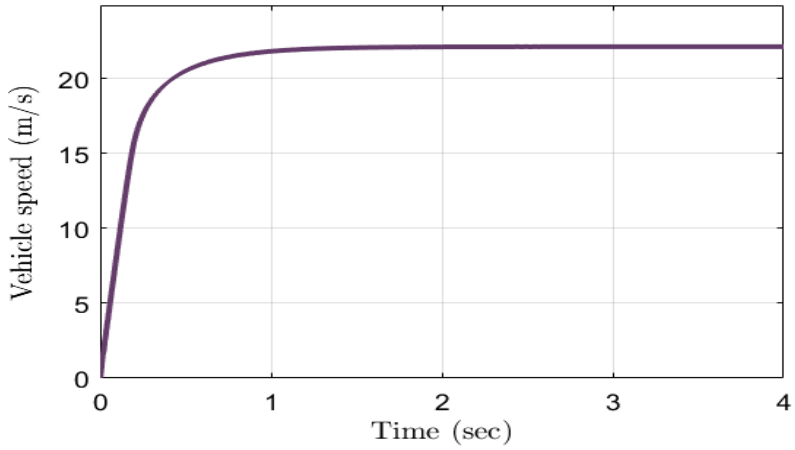

Figure 5.4 Response of the vehicle speed

5.4 Speed Control using PI Controller

The speed response for the PI controller without load and load torque are shown in Figure 5.5. For a three-phase SRM with a 2000 RPM desired value, the PI controller is reaching the steady state condition at the time of the 0.1 sec response of improved overshoots and rise time. The hysteresis current controller limits the phase current in a specified range and provides gate signals to the converter. After reaching the stable operating point, the steady-state error is also small. The peak overshoot is minimal when the speed is changed. In variable-speed drive applications, the system responds quickly and maintains a constant speed due to changes in load disturbance. Figure 5.5 shows a slightly significant change in speed in load variations. Likewise, the speed response and load torque are depicted in Figure 5.6 and Figure 5.7 respectively.

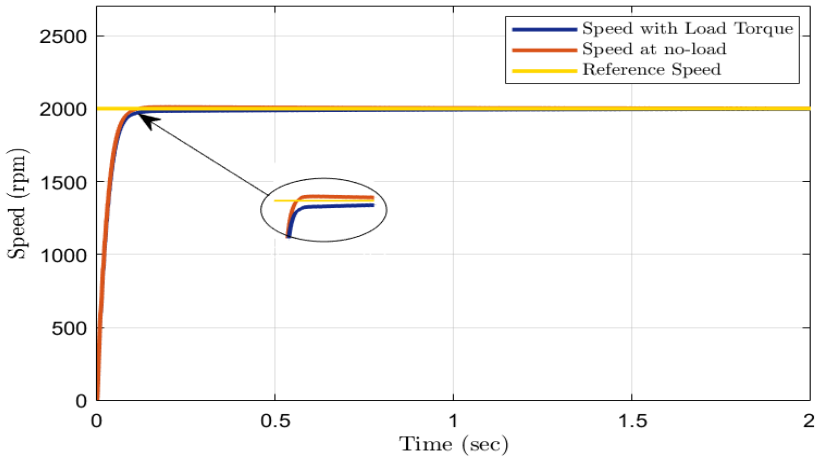

Figure 5.5 speed response of using PI control

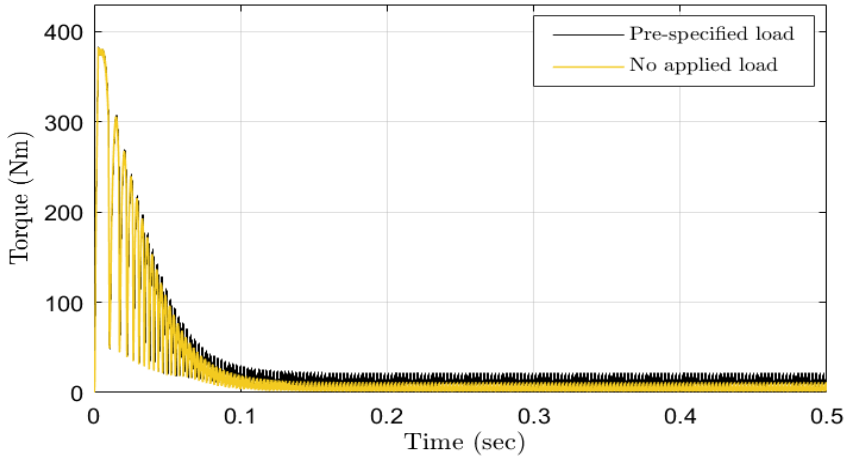

Figure 5.6 Response of torque using PI control

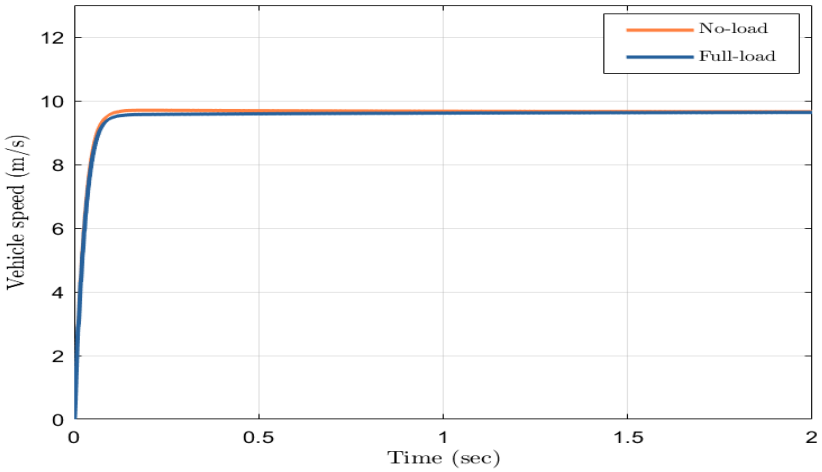

Figure 5.7 The response of the Vehicle speed using PI

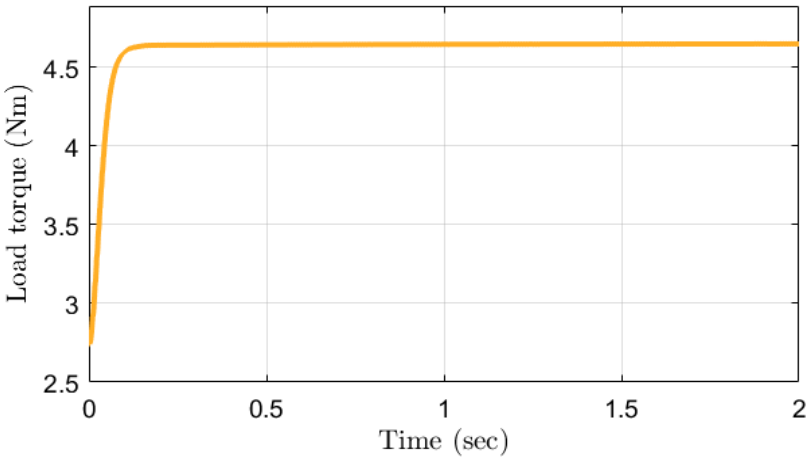

Figure 5.8 Load torque of the system

5.5 System Response of Fuzzy logic control using DTC

The designed system simulated for constant speed 2000 rpm with the flux reference of a motor of 0.35 Wb, the flux, and torque controller band limits are adjusted with ±0.486 Wb and ±0.001 Nm respectively. Table A.1 provides the SRM specifications. Various simulation results of the fuzzy logic controller and DTC using SRM are simulation results of DTC demonstrated in the different accompanying figures.

Figure 5.8 shows the speed output using the designed system Compared with fuzzy logic control. Using the DTC technique, the fuzzy logic controller enables the actual speed to follow closely with the reference speed in approximately 0.047 seconds. However, 0.098 seconds of rise time and 0.127 seconds of settling time were measured in FLC controller. The introduced designed controller 53.47% improves in faster response over conventional FLC. The motor speed and vehicle speed responses are shown in Figures 5.9 and 5.10 respectively.

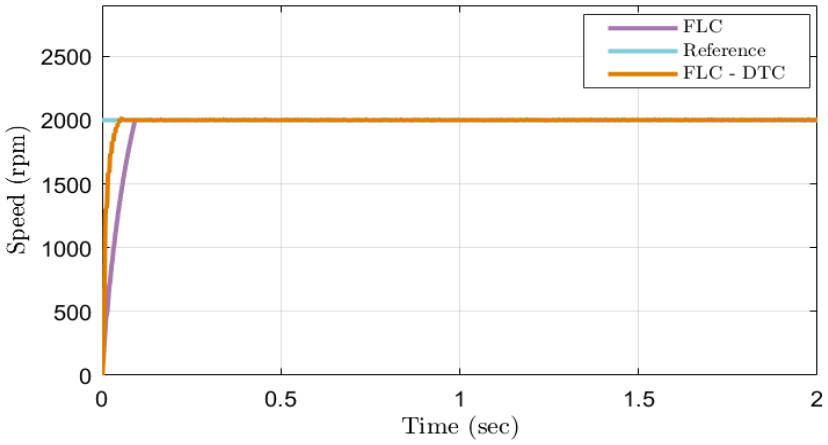

Figure 5.9 Speed response of designed controller

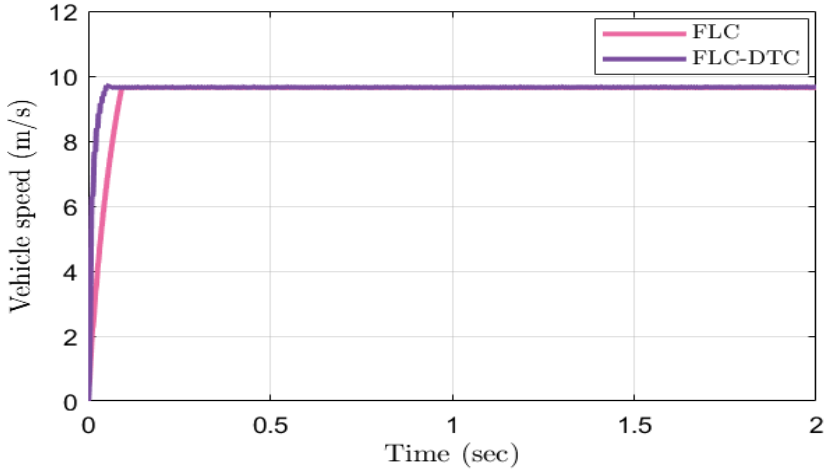

Figure 5.10 Response of the vehicle speed

Figure 5.11 displays the electromagnetic torque response, while Figure 5.12 reveals that the load torque reaches its lowest value. This minimal load torque condition permits the motor to accelerate, thereby increasing its rotational speed.

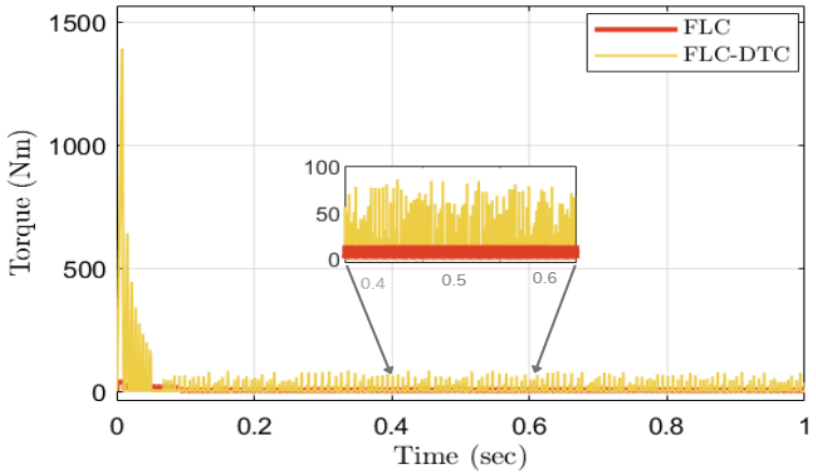

Figure 5.11 Torque response for the designed controller

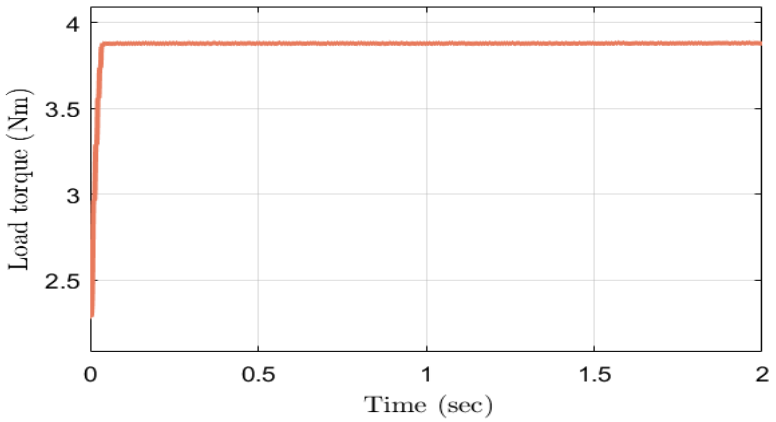

Figure 5.12 The load torque on the motor

The input of the motor is a battery that rates 91.6 A, and then the output current of the motor is depicted in Figure 5.13. The force generated by the vehicle power train that overcomes resistive forces and enables the vehicle to accelerate is shown in Figure 5.14. During the vehicle's in initial acceleration state, a high traction force is required to overcome inertia and net forces exerted on the vehicle. Once the vehicle attained a constant speed, the traction force reduced and diminished force stayed to opposing aerodynmic drag force and rolling resistance force.

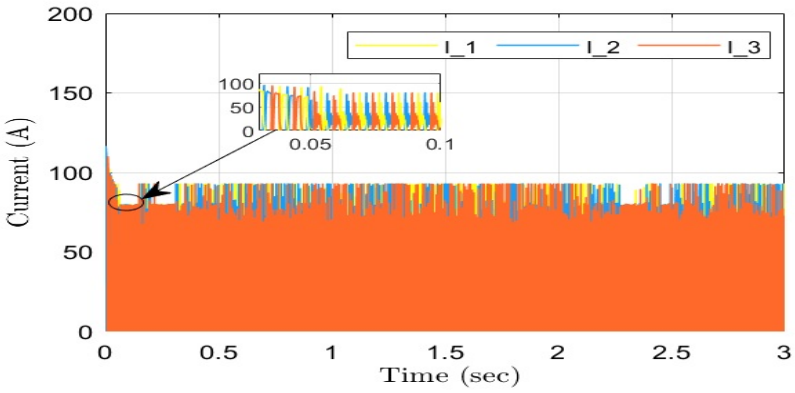

Figure 5.13 The output current of the motor

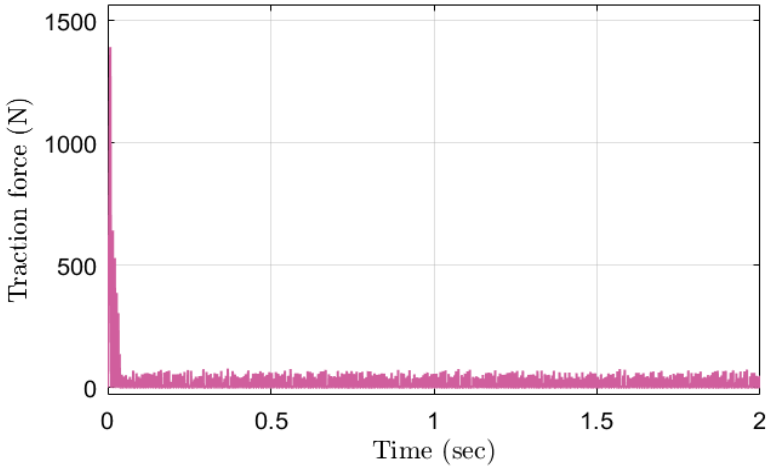

Figure 5.14 Traction force of the vehicle

The evaluation of PI, FLC, and FLC combined with DTC regarding rise time, settling time, and torque ripple percentage is shown in Table 5.1. It is evident from the table that the speed and dynamic responses are enhanced, resulting in reduced rise and settling times.

Table 5.1 Performance Comparison of Different Controllers

Controller	**Torque Ripple**	**Rise time (s)**	**Peak (rpm)**	**Settling time(s)**
PI	38%	0.112	2067	0.859
FLC	25%	0.098	2012	0.127
FLC with DTC	11%	0.047	2000	0.049

5.5.1 Responses for speed change and rapid speed reference variations

The designed controller is evaluated under a different speed change scenario. The rapid change in reference speed is evaluated and illustrated in Figure 5.15. The speed of the motor has been raised from 500 rpm to 1000 rpm with time t = 1s. During this circumstance, the designed controller was enhanced to keep the speed at the desired value. The speed of the vehicle for speed variation is presented in Figure 5.16. The designed controller is tested for different kinds of reference speed changes, and the motors enable them to operate according to the given rapid input variations. Figure 5.17 shows the capability of the motor for rapid reference speed variation.

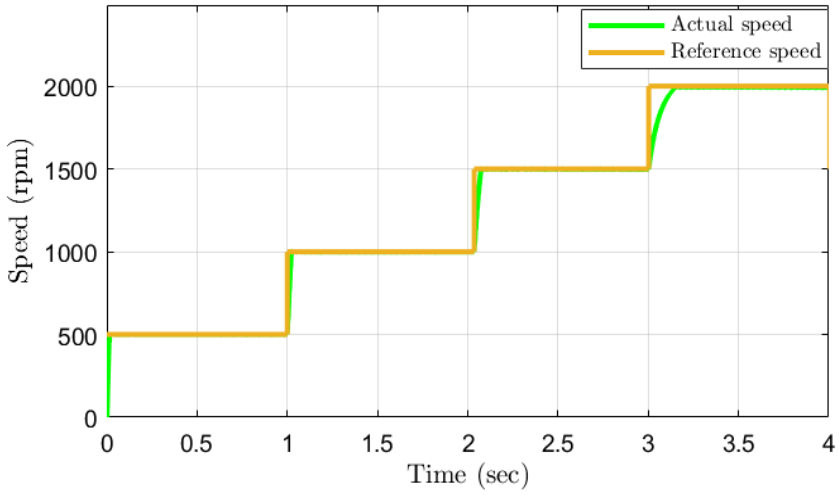

Figure 5.15 Variable speed response for the designed controller

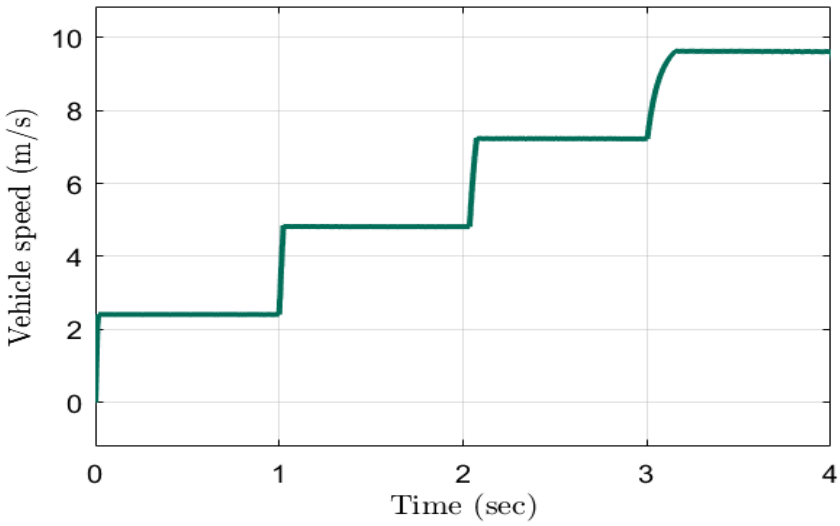

Figure 5.16 vehicle response for speed change

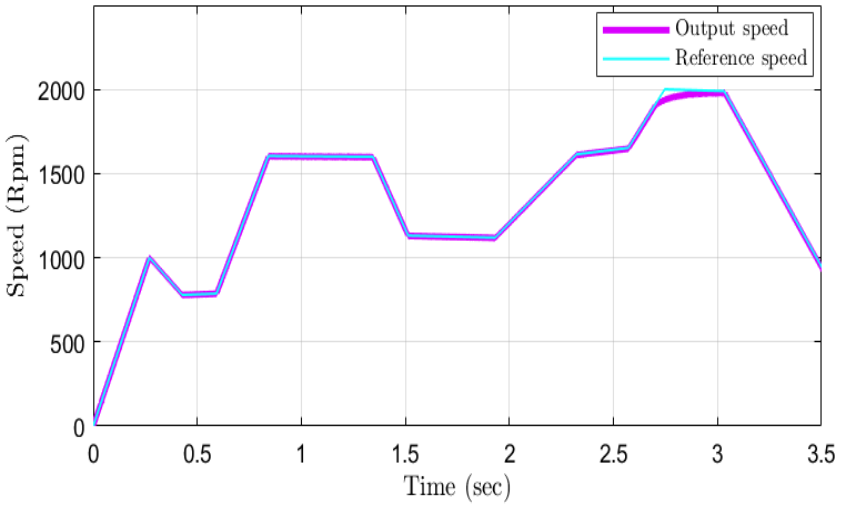

Figure 5.17 Motor response for rapid Reference speed variation

The speed responses for vehicle mass variation are demonstrated in Figure 5.18. For a prespecified mass of the vehicle the motor achieves its target speed in 0.047 seconds, while increasing the vehicle mass by 25% shows a moderate speed compared with a GVW speed and stabilizes at 0.097 seconds. At 50% mass, the motor struggles with inertia, taking 0.389 seconds to reach the 2000 RPM reference speed. The full (100%) mass configuration slows the acceleration and is highly opposed the delivered motor torque.

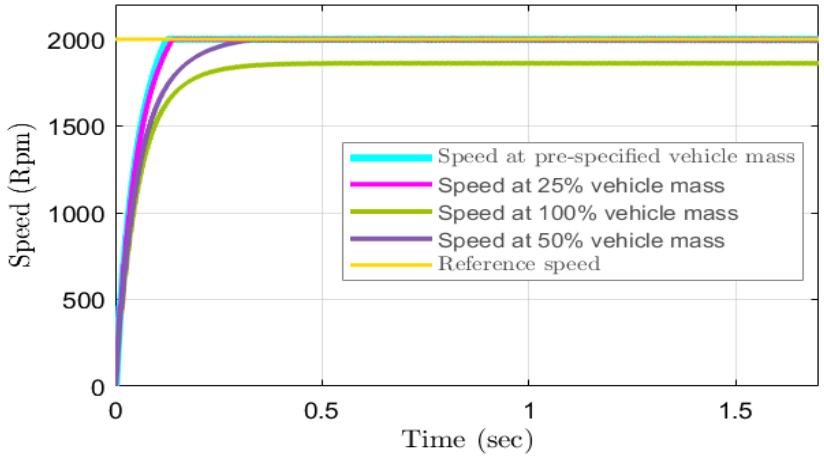

Figure 5.18 Motor speed response for vehicle mass variations

5.6 Simulink result for Power train model of EVs

To understand the data related to the battery, motor parameters, and forces acting on the vehicle powertrains modeled and depicted in Appendix B.1. The cell numbers in parallel and series which is useful for designing the battery pack, estimating how the resistive force

acts on the vehicle, the change in wheel speed, and speed of the motor requirement based on the effective gear ratios, and the battery pack remain after one complete cycle and battery capacity in Ah are detailly explained.

Figure 5.19 (a)-(d) outlines the forces acting on the vehicles. The acceleration force shown in Figure 5.19 (a) describes the deceleration when the speed drops from high speed to lower and the positive shows the strong acceleration. The aerodynamic force is similar according to the velocity profile input, due to it being proportional to the square of the velocity as elucidated in Figure 5.19 (c). The gradient force is zero due to there is no slope angle and the rolling resistance is constant as it does not depend on the velocity input as depicted in Figure 5.19 (b) and (d) respectively.

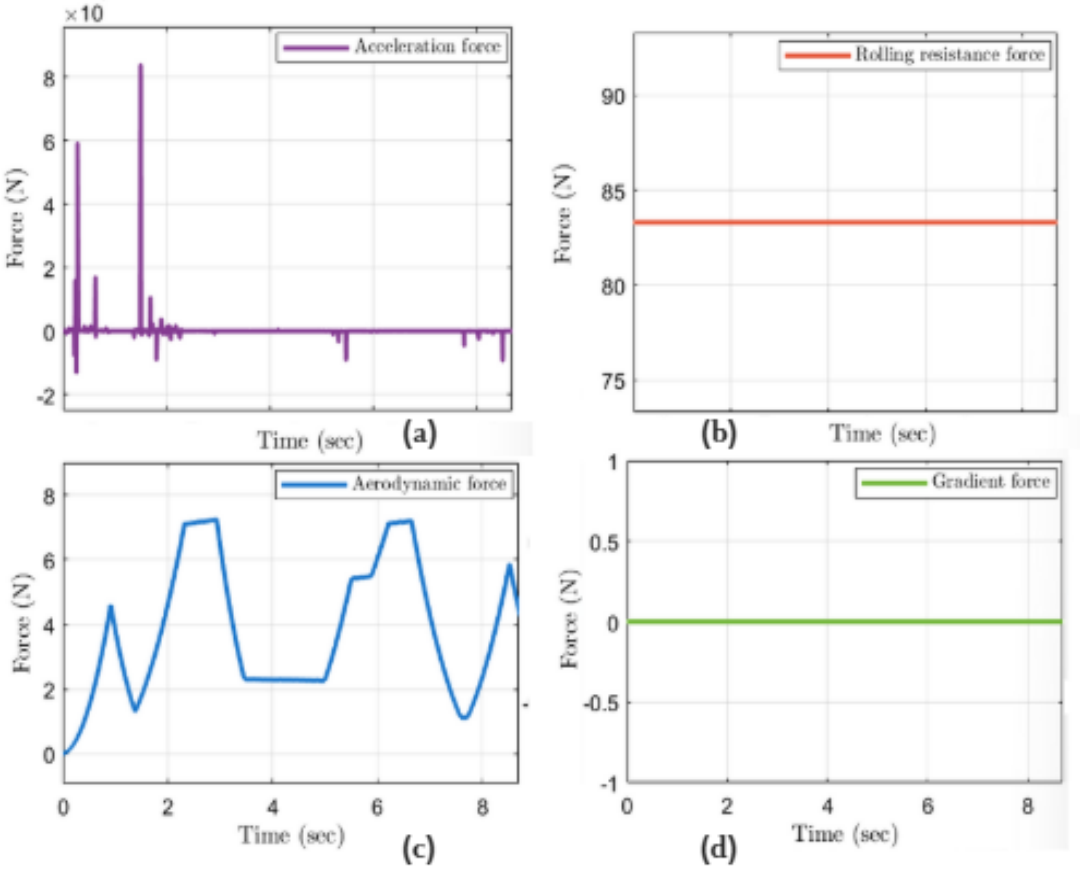

Figure 5.19 Traction force of : (a) Acceleration; (b) Rolling resistance; (c) Aerodynamic; and (d) Gradient

For the given velocity input, the wheel speed is around 148 RPM as depicted in Figure 5.20 (a), with the effective gear ratio from the motor capable of giving 800 RPM as a demonstration in Figure 5.20 (b). The vehicle speed response provided in Figure 5.20 (c) is a valuable top speed of 3.8 m/s.

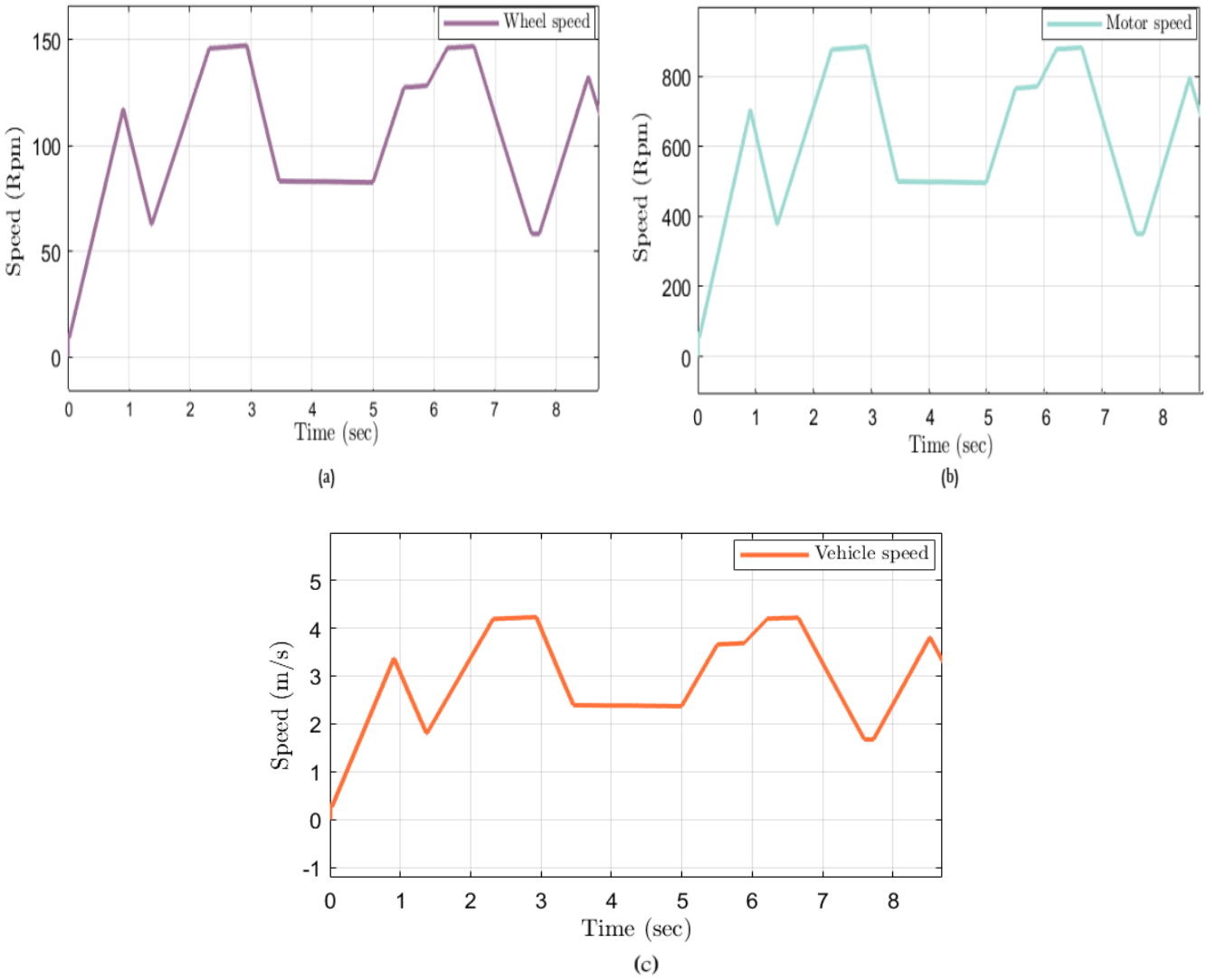

Figure 5.20 Speed response of (a) wheel; (b) motor; and (c) vehicle

The motor experienced a peak torque of 43 Nm at an operation speed of 800 RPM, and 22 Nm is the distributed torque on the wheels to meet the desired efficiency needs. Figure 5.21 exhibits the motor's electrical torque output alongside the torque demand required at the wheel. The analysis shows that accelerating the wheel to 120 RPM demands an initial high starting torque of 43 Nm. Following deceleration, the motor torque drops to zero and remains absent until the vehicle attains a speed of 4.2 m/s.

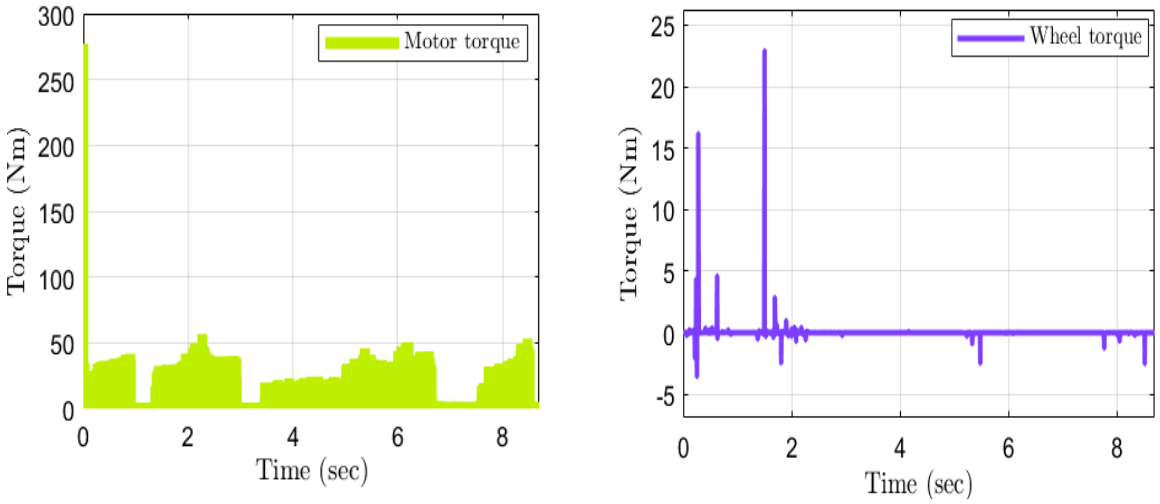

(a) (b)

Figure 5.21 Torque response of (a) motor and (b) vehicle

The state of charge remaing after completing the cycle is 99.85%, so around 0.15% of charge is used in one complete cycle and illustrated in Figure 5.22

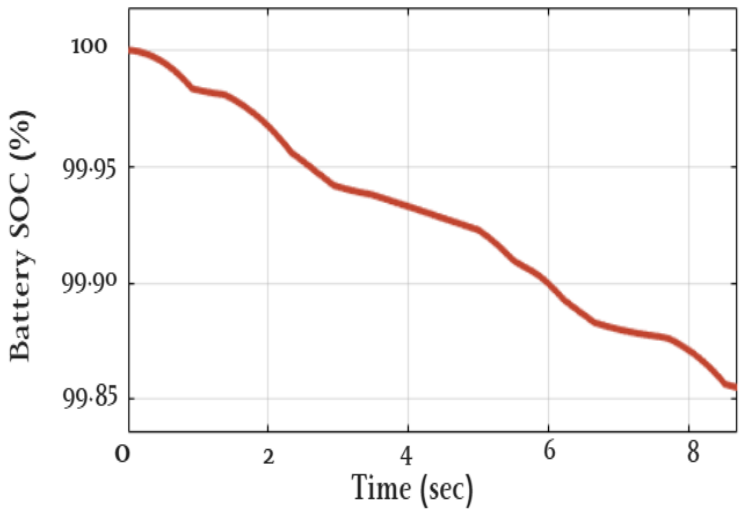

Figure 5.22 Battery SOC

Chapter 6

Conclusions and Recommendations

6.1 Conclusions

In this study, a fuzzy logic control (FLC) approach was developed to minimize torque ripple in electric vehicle (EV) applications while ensuring accurate speed tracking for switched reluctance motors (SRMs). The fuzzy logic controller was implemented using MATLAB software by integrating FLC with direct torque control (DTC) to regulate motor speed. The control system operates with two loops: an inner loop that manages torque to reduce ripple and an outer loop that utilizes FLC for motor speed regulation.
Based on the simulation results, the following conclusions were drawn:

- The proposed fuzzy logic controller with DTC significantly enhances system performance by improving speed tracking and minimizing torque ripple.

- The controller enables the actual speed to closely follow the reference speed within approximately 0.047 seconds, demonstrating a 53.47% improvement in rise time compared to conventional FLC methods. Moreover, the designed controller was enhanced during rapid speed reference variation to keep the speed at the desired value.

- For a three-phase SRM with a target speed of 2000 RPM, a higher electromagnetic torque of 22 Nm and 3.8 Nm load torque. which reaches its lowest value. This minimal load torque condition permits the motor to accelerate, thereby increasing its rotational speed

- Responses for rapid speed reference variations, a The speed of the motor has been raised from 500 rpm into 1000 rpm with time t = 1s. During this circumstance, the designed controller was enhanced to keep the speed with the desired value.

6.2 Recommendations

The results under different conditions demonstrate that the fuzzy logic-based DTC controller achieves faster reference speed tracking with reduced torque ripple, outperforming conventional controllers in both response time and speed stability. In this thesis, DTC compares the intended flux and torque values with the actual measured values and the switching table receives this control signal produced by hysteresis flux and torque control, but it is recommended to use intelligent control to avoid distortion in sector change and minimize sampling time.

Optimal torque production in switched reluctance motors (SRMs) relies on accurate rotor positioning. The disadvantage of position sensors is that they increase the size of the motor and additional manufacturing costs, which further reduces the efficiency and reliability of the system. So, sensor-less position control methods that implement the advanced control strategy are required.

Bibliography

[1] B. K. Bose, "Global warming: Energy, environmental pollution, and the impact of power electronics", *IEEE Industrial Electronics Magazine*, vol. 4, no. 1, pp. 6–17, 2010.

[2] E. Ferrero, S. Alessandrini, and A. Balanzino, "Impact of the electric vehicles on the air pollution from a highway", *Applied Energy*, vol. 169, pp. 450–459, May 2016. DOI: 10.1016/j.apenergy.2016.01.098.

[3] L. Cui, Y. Wang, W. Chen, W. Wen, and M. S. Han, "Predicting determinants of consumers' purchase motivation for electric vehicles: An application of maslow's hierarchy of needs model", *Energy Policy*, vol. 151, p. 112 167, 2021. [Online]. Available: https://api.semanticscholar.org/CorpusID:233589422.

[4] H. Cheng, Z. Wang, S. Yang, J. Huang, and X. Ge, "An integrated srm powertrain topology for plug-in hybrid electric vehicles with multiple driving and onboard charging capabilities", *IEEE Transactions on Transportation Electrification*, vol. 6, no. 2, pp. 578–591, 2020.

[5] Z. Darabi and M. Ferdowsi, "Aggregated impact of plug-in hybrid electric vehicles on electricity demand profile", *IEEE Transactions on Sustainable Energy*, vol. 2, no. 4, pp. 501–508, 2011.

[6] N. Zabihi and R. Gouws, "A review on switched reluctance machines for electric vehicles", in *2016 IEEE 25th International Symposium on Industrial Electronics (ISIE)*, 2016. DOI: 10.1109/ISIE.2016.7744992.

[7] G. V. Kumar, C.-H. Chuang, M.-Z. Lu, and C.-M. Liaw, "Development of an electric vehicle synchronous reluctance motor drive", *IEEE Transactions on Vehicular Technology*, vol. 69, no. 5, pp. 5012–5024, 2020.

[8] A. Rezig, W. Boudendouna, A. Djerdir, and A. N'Diaye, "Investigation of optimal control for vibration and noise reduction in-wheel switched reluctance motor used in

electric vehicle", *Mathematics and Computers in simulation*, vol. 167, pp. 267–280, 2020.

[9] B. Burkhart, A. Klein-Hessling, I. Ralev, C. P. Weiss, and R. W. De Doncker, "Technology, research and applications of switched reluctance drives", *CPSS Transactions on Power Electronics and Applications*, vol. 2, no. 1, pp. 12–27, 2017.

[10] V. F. Pires, A. J. Pires, A. Cordeiro, and D. Foito, "A review of the power converter interfaces for switched reluctance machines", *Energies*, vol. 13, no. 13, 2020, ISSN: 1996-1073. DOI: 10.3390/en13133490. [Online]. Available: https://www.mdpi.com/1996-1073/13/13/3490.

[11] S. Kudiyarasan, N. Sthalasayanam, and V. Karunakaran, "Minimization of torque pulsations by using a novel fuzzy controller in srm drives for ev applications", *Heliyon*, vol. 9, no. 3, e14437, 2023. DOI: 10.1016/j.heliyon.2023.e14437.

[12] M. Depenbrock, "Direct self-control of inverter fed machine", *IEEE Transactions on Power Electronics*, vol. 3, pp. 420–429, 1988. DOI: 10.1109/63.17963.

[13] I. Takahashi and T. Noguchi, "Take a look back upon the past decade of direct torque control [of induction motors]", *Proceedings of the IECON'97 23rd International Conference on Industrial Electronics, Control, and Instrumentation (Cat. No.97CH36066)*, vol. 2, 546–551 vol.2, 1997. [Online]. Available: https://api.semanticscholar.org/CorpusID:70364095.

[14] M. Waseem, G. S. Lakshmi, E. Sreeshobha, and S. Khan, "An electric vehicle battery and management techniques: Comprehensive review of important obstacles, new advancements, and recommendations", *Energy Storage and Saving*, 2024, ISSN: 2772-6835. DOI: https://doi.org/10.1016/j.enss.2024.09.002. [Online]. Available: https://www.sciencedirect.com/science/article/pii/S2772683524000384.

[15] Y. S. Wong and C. C. Chan, "Vehicle energy storagevehicleenergy storage: Batteriesvehicleenergy storagebatteries", in *Encyclopedia of Sustainability Science and Technology*, R. A. Meyers, Ed. New York, NY: Springer New York, 2012, pp. 11 502–11 522, ISBN: 978-1-4419-0851-3. DOI: 10.1007/978-1-4419-0851-3_808. [Online]. Available: https://doi.org/10.1007/978-1-4419-0851-3_808.

[16] B. E. Lebrouhi, S. Baghi, B. Lamrani, E. Schall, and T. Kousksou, "Critical materials for electrical energy storage: Li-ion batteries", *Journal of Energy Storage*, vol. 55, p. 105 471, 2022.

[17] T. Masese and G. M. Kanyolo, "The road to potassium-ion batteries", in *Storing Energy*, Elsevier, 2022, pp. 265–307.

[18] M. Al-Zareer, I. Dincer, and M. A. Rosen, "A thermal performance management system for lithium-ion battery packs", *Applied Thermal Engineering*, vol. 165, p. 114 378, 2020, ISSN: 1359-4311. DOI: https://doi.org/10.1016/j.applthermaleng.2019.114378. [Online]. Available: https://www.sciencedirect.com/science/article/pii/S1359431119336725.

[19] G. Zubi, R. Dufo-López, M. Carvalho, and G. Pasaoglu, "The lithium-ion battery: State of the art and future perspectives", *Renewable and Sustainable Energy Reviews*, vol. 89, pp. 292–308, 2018, ISSN: 1364-0321. DOI: https://doi.org/10.1016/j.rser.2018.03.002. [Online]. Available: https://www.sciencedirect.com/science/article/pii/S1364032118300728.

[20] J. A. Sanguesa, V. Torres-Sanz, P. Garrido, F. J. Martinez, and J. M. Marquez-Barja, "A review on electric vehicles: Technologies and challenges", *Smart Cities*, vol. 4, no. 1, pp. 372–404, 2021, ISSN: 2624-6511. DOI: 10.3390/smartcities4010022. [Online]. Available: https://www.mdpi.com/2624-6511/4/1/22.

[21] F. Un-Noor, S. Padmanaban, L. Mihet-Popa, M. N. Mollah, and E. Hossain, "A comprehensive study of key electric vehicle (ev) components, technologies, challenges, impacts, and future direction of development", *Energies*, vol. 10, no. 8, 2017, ISSN: 1996-1073. DOI: 10.3390/en10081217. [Online]. Available: https://www.mdpi.com/1996-1073/10/8/1217.

[22] O. Egbue and S. Long, "Barriers to widespread adoption of electric vehicles: An analysis of consumer attitudes and perceptions", *Energy Policy*, vol. 48, pp. 717–729, 2012, Special Section: Frontiers of Sustainability, ISSN: 0301-4215. DOI: https://doi.org/10.1016/j.enpol.2012.06.009. [Online]. Available: https://www.sciencedirect.com/science/article/pii/S0301421512005162.

[23] M. Li, Y. Bai, C. Zhang, *et al.*, "Review on the research of hydrogen storage system fast refueling in fuel cell vehicle", *International Journal of Hydrogen Energy*, vol. 44, no. 21, pp. 10 677–10 693, Apr. 2019. DOI: 10.1016/j.ijhydene.2019.02.208.

[24] F. Musavi and W. Eberle, "Overview of wireless power transfer technologies for electric vehicle battery charging", *IET Power Electronics*, vol. 7, no. 1, pp. 60–66, 2014. DOI: https://doi.org/10.1049/iet-pel.2013.0047. eprint: https://ietresearch.onlinelibrary.wiley.com/doi/pdf/10.1049/iet-pel.2013.0047. [Online]. Available: https://ietresearch.onlinelibrary.wiley.com/doi/abs/10.1049/iet-pel.2013.0047.

[25] U. D. of Energy. "How do all-electric cars work?" Accessed: 2025-02-19. (2023), [Online]. Available: https://afdc.energy.gov/vehicles/how-do-all-electric-cars-work.

[26] S. P. Kodali and S. Das, "Implementation of five level charging scheme in lithium-ion batteries for enabling fast charging in plug-in hybrid electric vehicles", in *2017 National Power Electronics Conference (NPEC)*, 2017, pp. 18–20.

[27] Y. Li and P. Han, "Multi-level charging control algorithm of electric vehicle in evs-grid system", in *2017 29th Chinese Control And Decision Conference (CCDC)*, IEEE, 2017, pp. 6965–6970.

[28] T. Chian, W. Wei, E. Ze, *et al.*, "A review on recent progress of batteries for electric vehicles", *International Journal of Applied Engineering Research*, vol. 14, no. 24, pp. 4441–4461, 2019.

[29] B. Kennedy, D. Patterson, and S. Camilleri, "Use of lithium-ion batteries in electric vehicles", *Journal of Power Sources*, vol. 90, no. 2, pp. 156–162, 2000.

[30] P. Bernard and M. Lippert, "Nickel–cadmium and nickel–metal hydride battery energy storage", in *Electrochemical energy storage for renewable sources and grid balancing*, Elsevier, 2015, pp. 223–251.

[31] C. Delmas, "Sodium and sodium-ion batteries: 50 years of research", *Advanced Energy Materials*, vol. 8, no. 17, p. 1 703 137, 2018.

[32] A. Mahmoudzadeh Andwari, A. Pesiridis, S. Rajoo, R. Martinez-Botas, and V. Esfahanian, "A review of battery electric vehicle technology and readiness levels", *Renewable and Sustainable Energy Reviews*, vol. 78, no. C, pp. 414–430, 2017. [Online]. Available: https://EconPapers.repec.org/RePEc:eee:rensus:v:78:y:2017:i:c:p:414-430.

[33] A. Khaligh and Z. Li, "Battery, ultracapacitor, fuel cell, and hybrid energy storage systems for electric, hybrid electric, fuel cell, and plug-in hybrid electric vehicles: State of the art", *IEEE Transactions on Vehicular Technology*, vol. 59, pp. 2806–2814, 2010. [Online]. Available: https://api.semanticscholar.org/CorpusID:271538.

[34] M. Zeraoulia, M. E. H. Benbouzid, and D. Diallo, "Electric motor drive selection issues for hev propulsion systems: A comparative study", *IEEE Transactions on Vehicular technology*, vol. 55, no. 6, pp. 1756–1764, 2006.

[35] A. Emadi, Y. J. Lee, and K. Rajashekara, "Power electronics and motor drives in electric, hybrid electric, and plug-in hybrid electric vehicles", *IEEE Transactions on industrial electronics*, vol. 55, no. 6, pp. 2237–2245, 2008.

[36] J. Urresty, J. Riba, M. Delgado, and L. Romeral, "Detection of demagnetization faults in surface-mounted permanent magnet synchronous motors by means of the zero-sequence voltage component", *IEEE transactions on energy conversion*, vol. 27, no. 1, pp. 42–51, Mar. 2012. DOI: 10.1109/TEC.2011.2176127. [Online]. Available: http://hdl.handle.net/2117/16262.

[37] Z. Yang, F. Shang, I. P. Brown, and M. Krishnamurthy, "Comparative study of interior permanent magnet, induction, and switched reluctance motor drives for ev and hev applications", *IEEE Transactions on Transportation Electrification*, vol. 1, no. 3, pp. 245–254, 2015.

[38] M. A. Hassanin, F. E. Abdel-Kader, S. I. Amer, and A. E. Abu-Moubarka, "Operation of brushless dc motor to drive the electric vehicle", in *2018 Twentieth International Middle East Power Systems Conference (MEPCON)*, IEEE, 2018, pp. 500–503.

[39] L. Ding and J. Song, "Comprehensive analysis of electric vehicles: State-of-arts and future aspects", *Highlights in Science, Engineering and Technology*, vol. 27, pp. 756–766, 2022. DOI: 10.54097/hset.v27i.3841. [Online]. Available: https://drpress.org/ojs/index.php/HSET/article/view/3841.

[40] I. Husain, B. Ozpineci, M. S. Islam, *et al.*, "Electric drive technology trends, challenges, and opportunities for future electric vehicles", *Proceedings of the IEEE*, vol. 109, no. 6, pp. 1039–1059, 2021.

[41] P. Ramesh and N. Lenin, "High power density electrical machines for electric vehicles—comprehensive review based on material technology", *IEEE Transactions on Magnetics*, vol. 55, no. 11, pp. 1–21, 2019.

[42] A. Chiba and K. Kiyota, "Review of research and development of switched reluctance motor for hybrid electrical vehicle", in *2015 IEEE workshop on electrical machines design, control and diagnosis (WEMDCD)*, IEEE, 2015, pp. 127–131.

[43] C. He, C. Hao, W. Qianlong, X. Shaohui, and Y. Shunyao, "Design and control of switched reluctance motor drive for electric vehicles", in *2016 14th International Conference on Control, Automation, Robotics and Vision (ICARCV)*, IEEE, 2016, pp. 1–6.

[44] S. Dey, B. Fernandes, and K. Chatterjee, "A novel magnetic gear integrated segmented rotor srm with reduced rare-earth material", in *2024 IEEE International Conference on Industrial Technology (ICIT)*, IEEE, 2024, pp. 1–6.

[45] C. Gong, S. Li, and T. Habetler, "High-strength rotor design for ultra-high speed switched reluctance machines", *IEEE Transactions on Industry Applications*, vol. 56, no. 2, pp. 1432–1442, 2020.

[46] K. Aiso, M. Takahashi, and K. Akatsu, "Study of high speed srm using vector control for electric vehicle", in *2019 10th International Conference on Power Electronics and ECCE Asia (ICPE 2019-ECCE Asia)*, IEEE, 2019, pp. 1–7.

[47] R. Muzzammel, O. A. Sajid, M. Manzoor, A. Qayyum, and A. Shahzad, "Simulation analysis of pi based switched reluctance motor", *Journal of Engineering Research and Reports*, vol. 3, no. 2, pp. 1–12, 2019.

[48] K. Nimisha and R. Senthilkumar, "Optimal tuning of pid controller for switched reluctance motor speed control using particle swarm optimization", in *2018 International Conference on Control, Power, Communication and Computing Technologies (ICCPCCT)*, IEEE, 2018, pp. 487–491.

[49] M. Divandari, B. Rezaie, and A. R. Noei, "Speed control of switched reluctance motor via fuzzy fast terminal sliding-mode control", *Computers & Electrical Engineering*, vol. 80, p. 106 472, 2019.

[50] R. Abdel-Fadil and L. Számel, "Fuzzy logic current control of switched reluctance motor for electric vehicles applications", *International Journal of Engineering and Information Systems (IJEAIS)*, vol. 2, no. 4, pp. 19–28, 2018.

[51] A. Rajendran and B. Karthik, "Design and analysis of fuzzy and pi controllers for switched reluctance motor drive", *Materials Today: Proceedings*, vol. 37, pp. 1608–1612, 2021.

[52] H. S. Hameed, Q. Al Azze, and M. S. Hasan, "Speed control of switched reluctance motors based on fuzzy logic controller and matlab/simulink", *Indonesian Journal of Electrical Engineering and Computer Science*, vol. 31, no. 2, pp. 647–657, 2023.

[53] Z. Xu, T. Li, F. Zhang, Y. Zhang, D.-H. Lee, and J.-W. Ahn, "A review on segmented switched reluctance motors", *Energies*, vol. 15, no. 23, 2022, ISSN: 1996-1073. DOI: 10.3390/en15239212. [Online]. Available: https://www.mdpi.com/1996-1073/15/23/9212.

[54] P. S. Melo and R. E. Araújo, "Switched reluctance motor modeling and loss estimation review", in *Modelling and Control of Switched Reluctance Machines*, R. E. Araújo and J. R. Camacho, Eds., Rijeka: IntechOpen, 2020, ch. 2. DOI: 10.5772/intechopen.92228. [Online]. Available: https://doi.org/10.5772/intechopen.92228.

[55] D. Xiao, J. Ye, G. Fang, Z. Xia, and A. Emadi, "Magnetic-characteristic-free high-speed position-sensorless control of switched reluctance motor drives with quadrature flux estimators", *IEEE Journal of Emerging and Selected Topics in Power Electronics*, vol. 10, no. 1, pp. 220–235, 2021.

[56] K. Youghourta, G. Abderrazak, and A. Arif, "6/4 srm electromagnetic modeling and control by using finite element method", in *2021 International Conference on Electrical, Communication, and Computer Engineering (ICECCE)*, IEEE, 2021, pp. 1–6.

[57] F. Al-Amyal, L. Számel, and M. Hamouda, "An enhanced direct instantaneous torque control of switched reluctance motor drives using ant colony optimization", *Ain Shams Engineering Journal*, vol. 14, no. 5, p. 101 967, 2023.

[58] J. Stephenson and J. Čorda, "Computation of torque and current in doubly salient reluctance motors from nonlinear magnetisation data", in *Proceedings of the Institution of Electrical Engineers*, IET, vol. 126, 1979, pp. 393–396.

[59] Z. Yu, C. Gan, Y. Chen, and R. Qu, "Dc-biased sinusoidal current excited switched reluctance motor drives based on flux modulation principle", *IEEE Transactions on Power Electronics*, vol. 35, no. 10, pp. 10 614–10 628, 2020.

[60] D. Lin, P. Zhou, S. Stanton, and Z. Cendes, "An analytical circuit model of switched reluctance motors", *IEEE Transactions on Magnetics*, vol. 45, no. 12, pp. 5368–5375, 2009.

[61] G. Fang, F. P. Scalcon, D. Xiao, R. P. Vieira, H. A. Gründling, and A. Emadi, "Advanced control of switched reluctance motors (srms): A review on current regulation, torque control and vibration suppression", *IEEE Open Journal of the Industrial Electronics Society*, vol. 2, pp. 280–301, 2021.

[62] R. Preethishri and J. A. Roseline, "Switched reluctance motor (srm) development by using matlab-simulink", in *2019 2nd International Conference on Power and Embedded Drive Control (ICPEDC)*, IEEE, 2019, pp. 152–157.

[63] E. Afjei, A. Siadatan, and M. Rafiee, "Construction of a low cost asymmetric bridge converter for switched reluctance motor drive", in *2013 21st Iranian Conference on Electrical Engineering (ICEE)*, IEEE, 2013, pp. 1–5.

[64] S. M. Mahmoud, M. Z. El-Sherif, E. S. Abdel-Aliem, and M. N. Nashed, "Studying different types of power converters fed switched reluctance motor", *International Journal of Electronics and Electrical Engineering*, vol. 1, no. 4, pp. 281–290, 2013.

[65] F. Un-Noor, S. Padmanaban, L. Mihet-Popa, M. N. Mollah, and E. Hossain, "A comprehensive study of key electric vehicle (ev) components, technologies, challenges, impacts, and future direction of development", *Energies*, vol. 10, no. 8, p. 1217, 2017.

[66] F. Naseri, E. Farjah, and T. Ghanbari, "An efficient regenerative braking system based on battery/supercapacitor for electric, hybrid, and plug-in hybrid electric vehicles with bldc motor", *IEEE Transactions on Vehicular Technology*, vol. 66, no. 5, pp. 3724–3738, 2016.

[67] A. Smallbone, B. Jia, P. Atkins, and A. P. Roskilly, "The impact of disruptive powertrain technologies on energy consumption and carbon dioxide emissions from heavy-duty vehicles", *Energy Conversion and Management: X*, vol. 6, p. 100 030, 2020, ISSN: 2590-1745. DOI: https://doi.org/10.1016/j.ecmx.2020.100030. [Online]. Available: https://www.sciencedirect.com/science/article/pii/S2590174520300027.

[68] A. K. Maurya, "Design and fabrication of a prototype electric vehicle", *AKGEC International Journal of Technology*, vol. 12, no. 1, 2021.

[69] F. Naseri, C. Barbu, and T. Sarikurt, "Optimal sizing of hybrid high-energy/high-power battery energy storage systems to improve battery cycle life and charging power in electric vehicle applications", *Journal of Energy Storage*, vol. 55, p. 105 768, 2022, ISSN: 2352-152X. DOI: https://doi.org/10.1016/j.est.2022.105768. [Online]. Available: https://www.sciencedirect.com/science/article/pii/S2352152X2201756X.

[70] F. Naseri, C. Barbu, and T. Sarikurt, "Optimal sizing of hybrid high-energy/high-power battery energy storage systems to improve battery cycle life and charging power in electric vehicle applications", *Journal of Energy Storage*, vol. 55, p. 105 768, 2022.

[71] S. Manzetti and F. Mariasiu, "Electric vehicle battery technologies: From present state to future systems", *Renewable and Sustainable Energy Reviews*, vol. 51, pp. 1004–1012, 2015.

[72] N. Nitta, F. Wu, J. T. Lee, and G. Yushin, "Li-ion battery materials: Present and future", *Materials today*, vol. 18, no. 5, pp. 252–264, 2015.

[73] M. Boutouba, A. El Ougli, S. Miqoi, and B. Tidhaf, "Asymmetric fuzzy logic controlled dc-dc converter for solar energy system", *Renewable Energy and Sustainable Development*, vol. 2, no. 1, pp. 52–59, 2016.

[74] A. A. Abdel-Aziz, K. H. Ahmed, A. M. Massoud, and B. W. Williams, "Unaligned inductance calculation using flux tube approach for rotor conducting screen-based srm", *IET Electric Power Applications*, vol. 15, no. 8, pp. 1081–1094, 2021.

[75] V. Pushparajesh and B. Nandish, "Classical direct torque control for switched reluctance motor drive", in *New Trends in Electric Machines*, M. Delgado-Prieto, J. A. A. Daviu, and R. A. O. Rios, Eds., Rijeka: IntechOpen, 2022, ch. 5. DOI: 10.5772/intechopen.107876. [Online]. Available: https://doi.org/10.5772/intechopen.107876.

Appendix A

The 6/4 SRM parameters from MATLAB/Simulink Library is outlined in below table.

Table A.1 Motor Specification

Parameter	**Symbol**
No. of stator poles	6
No. of rotor poles	4
No. of phases	3
Stator resistance	0.05 ohm/phase
Friction	0.001 N·m·s
Inertia	0.05 kg·m^2
Inertia position and speed	0 rad,0 m/s
Unaligned inductance	0.6 mH
Aligned inductance	23 mH
Saturated aligned inductance	0.15mH
Maximum current	450 A
Maximum flux linkage	0.486 Weber-turn

Appendix B

B.1

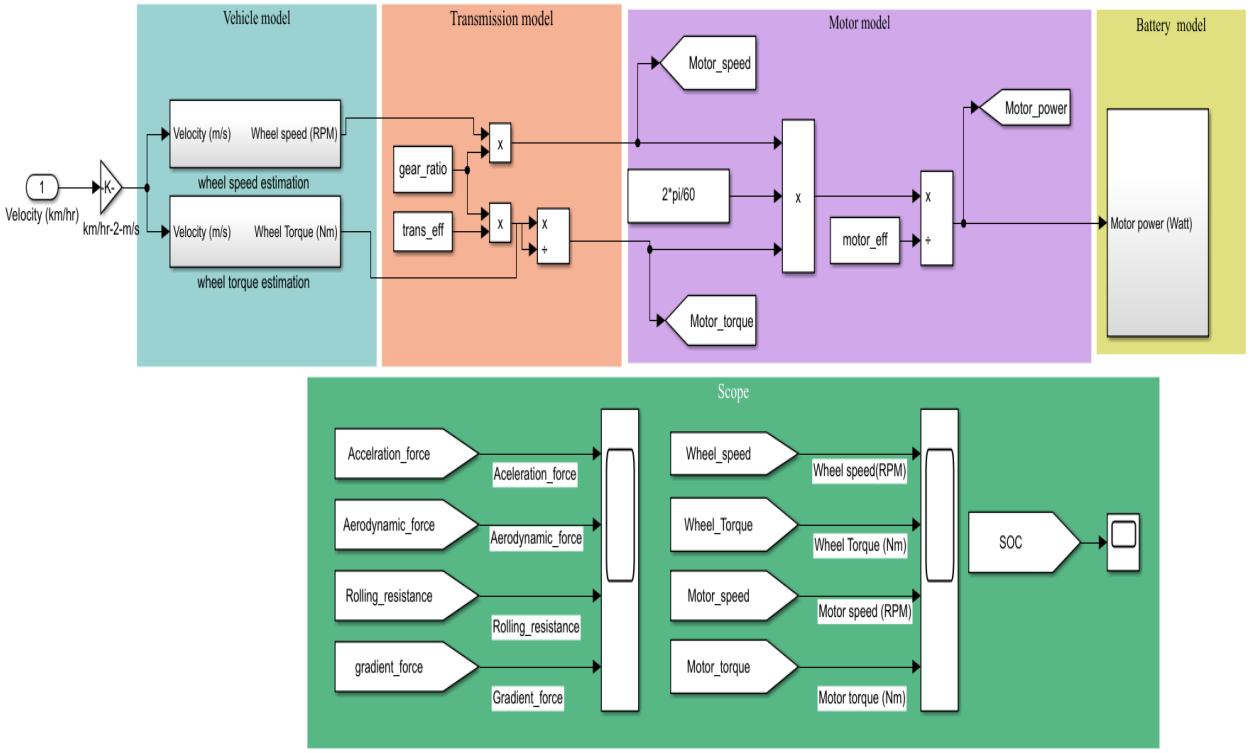

Figure B.1 Simulink model of EV Power train model

B.2

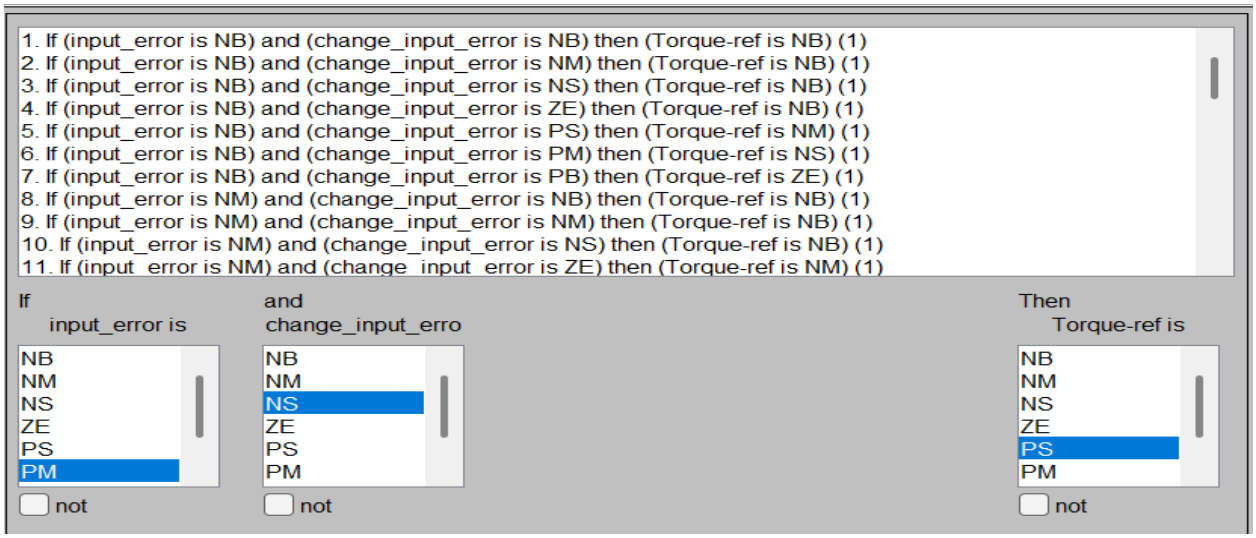

Figure B.2 Rule editor graphics